Residual-based a posteriori error analysis for symmetric mixed Arnold–Winther FEM

Carsten Carstensen[1] · Dietmar Gallistl[2] · Joscha Gedicke[3]

Abstract

This paper introduces an explicit residual-based a posteriori error analysis for the symmetric mixed finite element method in linear elasticity after Arnold–Winther with pointwise symmetric and $H(\mathrm{div})$-conforming stress approximation. The residual-based a posteriori error estimator of this paper is reliable and efficient and truly explicit in that it solely depends on the symmetric stress and does neither need any additional information of some skew symmetric part of the gradient nor any efficient approximation thereof. Hence, it is straightforward to implement an adaptive mesh-refining algorithm. Numerical experiments verify the proven reliability and efficiency of the new a posteriori error estimator and illustrate the improved convergence rate in comparison to uniform mesh-refining. A higher convergence rate for piecewise affine data is observed in the L^2 stress error and reproduced in non-smooth situations by the adaptive mesh-refining strategy.

Mathematics Subject Classification 65N15 · 65N30

✉ Joscha Gedicke
   joscha.gedicke@univie.ac.at

   Carsten Carstensen
   cc@math.hu-berlin.de

   Dietmar Gallistl
   d.gallistl@utwente.nl

[1] Humboldt-Universität zu Berlin, Berlin, Germany

[2] University of Twente, Enschede, The Netherlands

[3] Faculty of Mathematics, University of Vienna, Vienna, Austria

1 Introduction

1.1 Overview

The design of a pointwise symmetric stress approximation $\sigma_h \in L^2(\Omega; \mathbb{S})$ with divergence in $L^2(\Omega; \mathbb{R}^d)$, written $\sigma_h \in H(\text{div}, \Omega; \mathbb{S})$, has been a long-standing challenge [2] and the first positive examples in [5] initiated what nowadays is called the finite element exterior calculus [4]. The a posteriori error analysis of mixed finite element methods in elasticity started with [11] on PEERS [3], where the asymmetric stress approximation γ_h arises in the discretization as a Lagrange multiplier to enforce weakly the stress symmetry. This allows the treatment of the term $\mathbb{C}^{-1}\sigma_h + \gamma_h$ as an approximation of the (nonsymmetric) functional matrix Du for the displacement field [11] with the arguments of [1,9] developed for mixed finite element schemes for a Poisson model problem. Here and throughout, $\mathbb{C}$ denotes a fourth-order elasticity tensor with two Lamé constants λ and μ and $\mathbb{C}^{-1}$ is its inverse. Mixed finite element methods appear attractive in the incompressible limit for they typically avoid the locking phenomenon [12] as $\lambda \to \infty$.

For mixed finite element methods like the symmetric Arnold–Winther finite element schemes [5], the subtle term is the nonconforming residual: Given any piecewise polynomial $\sigma_h \in H(\text{div}, \Omega; \mathbb{S})$, compute an upper bound $\eta(\mathscr{T}, \sigma_h)$ of

$$\inf_{v \in V} \left\| \mathbb{C}^{-1/2}\sigma_h - \mathbb{C}^{1/2}\varepsilon(v) \right\|_{L^2(\Omega)} \lesssim \eta(\mathscr{T}, \sigma_h).$$

Despite general results in this direction [10,17,18], this task had been addressed only by the computation of an approximation to the optimal v with Green strain $\varepsilon(v) := \text{sym } Dv$ or of some skew-symmetric approximation γ_h motivated from the first results in [11] on PEERS. In fact, *any* choice of a piecewise smooth and pointwise skew-symmetric γ_h allows for an a posteriori error control of the symmetric stress error $\sigma - \sigma_h$ in [15]. Its efficiency, however, depends on the (unknown and uncontrolled) efficiency of the choice of γ_h as an approximation to the skew-symmetric part γ of Du.

This paper proposes the first reliable and efficient *explicit* residual-based a posteriori error estimator of the nonconforming residual with the typical contributions to $\eta(\mathscr{T}, \sigma_h)$ computed from the (known) Green strain approximation $\varepsilon_h := \mathbb{C}^{-1}\sigma_h$. Besides oscillations of the applied forces in the volume and along the Neumann boundary, there is a volume contribution $h_T^2 \| \text{rot rot } \varepsilon_h \|_{L^2(T)}$ for each triangle $T \in \mathscr{T}$ and an edge contribution with the jump $[\varepsilon_h]_E$ across an interior edge E with unit normal ν_E, tangential unit vector τ_E, and length h_E, namely

$$h_E^{1/2} \| \tau_E \cdot [\varepsilon_h]_E \tau_E \|_{L^2(E)} + h_E^{3/2} \| \tau_E \cdot [\text{rot}_{NC}\, \varepsilon_h]_E - \partial(\nu_E \cdot [\varepsilon_h]_E \tau_E)/\partial s \|_{L^2(E)},$$

and corresponding modification on the edges on the Dirichlet boundary with the (possibly inhomogeneous) Dirichlet data; cf. Remark 2 for some partial simplification of the last term displayed.

The analysis is restricted to the two dimensional case, since it involves explicit calculations in two dimensions without any reference to the exterior calculus but with

inhomogeneous Dirichlet and Neumann boundary data. The main result is reliability and efficiency to control the stress error robustly in the sense that the multiplicative generic constants hidden in the notation $\lesssim$ do neither depend on the (local or global) mesh-size nor on the parameter $\lambda > 0$ but may depend on $\mu > 0$ and on the shape regularity of the underlying triangulation $\mathscr{T}$ of the domain Ω into triangles through a lower bound of the minimal angle therein.

1.2 Linear elastic model problem

The elastic body Ω is a simply-connected bounded Lipschitz domain $\Omega \subset \mathbb{R}^2$ in the plane with a (connected) polygonal boundary $\partial\Omega = \Gamma_D \cup \Gamma_N$ split into parts. The displacement boundary Γ_D is compact and of positive surface measure, while the traction boundary is the relative open complement $\Gamma_N = \partial\Omega \backslash \Gamma_D$ with outer unit normal vector ν. Given $u_D \in H^1(\Omega; \mathbb{R}^2)$, the volume force $f \in L^2(\Omega; \mathbb{R}^2)$, and the applied surface traction $g \in L^2(\Gamma_N; \mathbb{R}^2)$, the linear elastic problem seeks a displacement $u \in H^1(\Omega; \mathbb{R}^2)$ and a symmetric stress tensor $\sigma \in H(\mathrm{div}, \Omega; \mathbb{S})$ with

$$
\begin{aligned}
-\operatorname{div} \sigma = f \quad &\text{and} \quad \sigma = \mathbb{C}\varepsilon(u) \quad \text{in } \Omega, \\
u = u_D \quad \text{on } \Gamma_D, \qquad &\sigma\nu = g \quad \text{on } \Gamma_N.
\end{aligned}
\tag{1}
$$

Throughout this paper, given the Lamé parameters $\lambda, \mu > 0$ for isotropic linear elasticity, the positive definite fourth-order elasticity tensor $\mathbb{C}$ acts as $\mathbb{C}E := 2\mu E + \lambda \operatorname{tr}(E) 1_{2\times 2}$ on any matrix $E \in \mathbb{S}$ with trace $\operatorname{tr}(E)$ and the 2×2 unit matrix $1_{2\times 2}$. Note that u_D acts in (1) only on Γ_D and is an extension of the continuous function $u_D \in C(\Gamma_D; \mathbb{R}^2)$ also supposed to belong to the edgewise second order Sobolev space $H^2(\mathscr{E}(\Gamma_D))$ below to allow second derivatives with respect to the arc length along boundary edges.

More essential will be a discussion on the precise conditions on the Neumann data g and its discrete approximation g_h below for they belong to the essential boundary conditions in the mixed finite element method based on the dual formulation.

In addition to the set of homogeneous displacements V and the aforementioned stress space $H(\mathrm{div}, \Omega; \mathbb{S})$, namely,

$$
\begin{aligned}
V &:= \{v \in H^1(\Omega; \mathbb{R}^2) \mid v|_{\Gamma_D} = 0\}, \\
H(\mathrm{div}, \Omega; \mathbb{S}) &:= \{\tau \in L^2(\Omega; \mathbb{S}) \mid \operatorname{div}\tau \in L^2(\Omega; \mathbb{R}^2)\},
\end{aligned}
$$

and with the exterior unit normal vector ν along $\partial\Omega$, the inhomogeneous stress space

$$
\Sigma(g) := \left\{ \sigma \in H(\mathrm{div}, \Omega; \mathbb{S}) \mid \int_{\Gamma_N} \psi \cdot (\sigma\nu)\, ds = \int_{\Gamma_N} \psi \cdot g\, ds \text{ for all } \psi \in V \right\}
$$

is defined with respect to the Neumann data $g \in L^2(\Gamma_N)$ and, in particular, $\Sigma_0 := \Sigma(0)$ abbreviates the stress space with homogeneous Neumann boundary conditions.

Given data u_D, f, g as before, the dual weak formulation of (1) seeks $(\sigma, u) \in \Sigma(g) \times L^2(\Omega; \mathbb{R}^2)$ with

$$\int_\Omega \sigma : \mathbb{C}^{-1}\tau \, dx + \int_\Omega u \cdot \operatorname{div} \tau \, dx = \int_{\Gamma_D} u_D \cdot (\tau\nu) \, ds \quad \text{for all } \tau \in \Sigma_0,$$

$$\int_\Omega v \cdot \operatorname{div} \sigma \, dx = -\int_\Omega f \cdot v \, dx \quad \text{for all } v \in L^2(\Omega; \mathbb{R}^2). \tag{2}$$

It is well known that the two formulations are equivalent and well posed in the sense that they allow for unique solutions in the above spaces and are actually slightly more regular according to the reduced elliptic regularity theory. The reader is refereed to textbooks on finite element methods [6–8] for proofs and further descriptions.

Throughout this paper, the model problem considers truly mixed boundary conditions with the hypothesis that both Γ_D and Γ_N have positive length. The remaining cases of a pure Neumann problem or a pure Dirichlet problem require standard modification and are immediately adopted. The presentation focuses on the case of isotropic linear elasticity with constant Lamé parameters λ and μ for brevity and many results carry over to more general situations (cf. Remarks 1 and 2 for instance).

1.3 Mixed finite element discretization

Let $\mathscr{T}$ denote a shape-regular triangulation of Ω into triangles (in the sense of Ciarlet [8]) with set of nodes $\mathscr{N}$, set of interior edges $\mathscr{E}(\Omega)$, set of Dirichlet edges $\mathscr{E}(\Gamma_D)$ and set of Neumann edges $\mathscr{E}(\Gamma_N)$. The triangulation is compatible with the boundary pieces Γ_D and Γ_N in that the boundary condition changes only at some vertex $\mathscr{N}$ and Γ_D (resp. $\overline{\Gamma_N}$) is partitioned in $\mathscr{E}(\Gamma_D)$ (resp. $\mathscr{E}(\Gamma_N)$).

The piecewise polynomials (piecewise with respect to the triangulation $\mathscr{T}$) of total degree at most $k \in \mathbb{N}_0$ are denoted as $P_k(\mathscr{T})$, their vector- or matrix-valued versions as $P_k(\mathscr{T}; \mathbb{R}^2)$ or $P_k(\mathscr{T}; \mathbb{R}^{2\times 2})$ etc. The subordinated Arnold–Winther finite element space $AW_k(\mathscr{T})$ of index $k \in \mathbb{N}$ [5] reads

$$AW_k(\mathscr{T}) := \left\{ \tau \in P_{k+2}(\mathscr{T}; \mathbb{S}) \cap H(\operatorname{div}, \Omega; \mathbb{S}) \,\middle|\, \operatorname{div} \tau \in P_k(\mathscr{T}; \mathbb{R}^2) \right\}.$$

The Neumann boundary conditions are essential conditions and are traditionally implemented by some approximation g_h to g in the normal trace space

$$G(\mathscr{T}) := \left\{ (\tau_h \nu)|_{\Gamma_N} \in L^2(\Gamma_N; \mathbb{R}^2) \,\middle|\, \tau_h \in AW_k(\mathscr{T}) \right\}$$

(recall that ν is the exterior unit normal along the boundary). Given any $g_h \in G(\mathscr{T})$, the discrete stress approximations are sought in the non-void affine subspace

$$\Sigma(g_h, \mathscr{T}) := \Sigma(g_h) \cap AW_k(\mathscr{T})$$

of $AW_k(\mathscr{T})$ with test functions in the linear subspace $\Sigma(0, \mathscr{T}) := \Sigma_0 \cap AW_k(\mathscr{T})$. Then there exists a unique discrete solution $\sigma_h \in \Sigma(g_h, \mathscr{T})$ and $u_h \in V_h := P_k(\mathscr{T}; \mathbb{R}^2)$ to

$$\int_\Omega \sigma_h : \mathbb{C}^{-1}\tau_h \, dx + \int_\Omega u_h \cdot \operatorname{div} \tau_h \, dx = \int_{\Gamma_D} u_D \cdot (\tau_h \nu) \, ds \quad \text{for all } \tau_h \in \Sigma(0, \mathscr{T}),$$

$$\int_\Omega v_h \cdot \operatorname{div} \sigma_h \, dx = \int_\Omega f \cdot v_h \, dx \quad \text{for all } v_h \in V_h.$$

$$\tag{3}$$

The explicit design of a Fortin projection leads in [5] to quasi-optimal a priori error estimates for an exact solution $(\sigma, u) \in (\Sigma(g) \cap H^{k+2}(\Omega; \mathbb{S})) \times H^{k+2}(\Omega)$ to (1) and the approximate solution (σ_h, u_h) to (3), namely (with the maximal mesh-size h)

$$\|\sigma - \sigma_h\|_{L^2(\Omega)} \lesssim h^m \|\sigma\|_{H^m(\Omega)} \quad \text{for } 1 \le m \le k + 2,$$

$$\|u - u_h\|_{L^2(\Omega)} \lesssim h^m \|u\|_{H^{m+1}(\Omega)} \quad \text{for } 1 \le m \le k + 1.$$

Another stable pair of different and mesh-depending norms in [14] implies the L^2 best approximation of the stress error $\sigma - \sigma_h$ up to a generic multiplicative constant and data oscillations on f under some extra condition (N) on the Neumann data approximation g_h implied by the first and zero moment orthogonality assumption $g - g_h \perp P_1(\mathscr{E}(\Gamma_N); \mathbb{R}^2)$ ($\perp$ indicates orthogonality in $L^2(\Gamma_N)$) met in all the numerical examples of this paper.

For simple benchmark examples with piecewise polynomial data f and g, there is even a superconvergence phenomenon visible in numerical examples. The arguments of this paper allow a proof of fourth-order convergence of the L^2 stress error $\|\sigma - \sigma_h\| = \mathcal{O}(h^4)$ in the lowest-order Arnold–Winther method with $k = 1$ for a smooth stress $\sigma \in H^4(\Omega; \mathbb{S})$ with $f = f_h \in P_1(\mathscr{T}; \mathbb{R}^2)$ and $g = g_h \in G(\mathscr{T})$. (In fact, once the data are not piecewise affine, the arising oscillation terms are only of at most third order and the aforementioned convergence estimates are sharp.)

This is stated as Theorem 5 in the appendix, because the a priori error analysis lies outside of the main focus of this work. It is surprising though that adaptive mesh-refining suggested with this paper recovers this higher convergence rate even for the inconsistent Neumann data in the Cook membrane benchmark example below.

1.4 Explicit residual-based a posteriori error estimator

The novel explicit residual-based error estimator for the discrete solution (σ_h, u_h) to (3) depends only on the Green strain approximation $\mathbb{C}^{-1}\sigma_h$ and its piecewise derivatives and jumps across edges.

Given any edge E of length h_E, let ν_E denote the unit normal vector (chosen with a fixed orientation such that it points outside along the boundary $\partial\Omega$ of Ω) and let τ_E denote its tangential unit vector; by convention $\tau_E = (0, -1; 1, 0)\nu_E$ with the indicated asymmetric 2×2 matrix. The tangential derivative $\tau_E \cdot \nabla\bullet$ along an edge (or boundary) is identified with the one-dimensional derivative $\partial \bullet / \partial s$ with respect to the arc-length parameter s. The jump $[v]_E$ of any piecewise continuous scalar, vector, or matrix v across an interior edge $E = \partial T_+ \cap \partial T_-$ shared by the two triangles T_+ and T_- such that ν_E points outside T_+ along $E \subset \partial T_+$ reads

$$[v]_E := (v|_{T_+})|_E - (v|_{T_-})|_E.$$

The rotation acts on a vector field Φ (and row-wise on matrices) via $\operatorname{rot}\Phi := \partial_1\Phi_2 - \partial_2\Phi_1$ and rot_{NC} denotes its piecewise application.

Under the present notation and the throughout abbreviation $\boldsymbol{\varepsilon}_h := \mathbb{C}^{-1}\sigma_h$, the explicit residual-based a posteriori error estimator reads

$$
\begin{aligned}
\eta^2 & (\mathcal{T}, \sigma_h) \\
& := \sum_{T\in\mathcal{T}} h_T^4 \|\operatorname{rot}\operatorname{rot}\boldsymbol{\varepsilon}_h\|_{L^2(T)}^2 + \operatorname{osc}^2(f,\mathcal{T}) + \operatorname{osc}^2(g - g_h, \mathcal{E}(\Gamma_N)) \\
& + \sum_{E\in\mathcal{E}(\Omega)} \left(h_E \|\tau_E \cdot [\boldsymbol{\varepsilon}_h]_E \tau_E\|_{L^2(E)}^2 + h_E^3 \|\tau_E \cdot \left([\operatorname{rot}_{NC}\boldsymbol{\varepsilon}_h]_E - \frac{\partial[\boldsymbol{\varepsilon}_h]_E\nu_E}{\partial s}\right)\|_{L^2(E)}^2 \right) \\
& + \sum_{E\in\mathcal{E}(\Gamma_D)} \left(h_E \|\tau_E \cdot \left(\boldsymbol{\varepsilon}_h\tau_E - \frac{\partial u_D}{\partial s}\right)\|_{L^2(E)}^2 + h_E^3 \|\tau_E \cdot \operatorname{rot}\boldsymbol{\varepsilon}_h - \nu_E \cdot \left(\frac{\partial\boldsymbol{\varepsilon}_h\tau_E}{\partial s} - \frac{\partial^2 u_D}{\partial s^2}\right)\|_{L^2(E)}^2 \right)
\end{aligned}
\tag{4}
$$

for the oscillations $\operatorname{osc}(f,\mathcal{T})$ of the volume force and the oscillations of the traction boundary condition $\operatorname{osc}(g - g_h, \mathcal{E}(\Gamma_N))$, defined below.

Theorem 1 (reliability) *There exists a mesh-size and λ independent constant C_{rel} (which may depend on μ and on the shape-regularity of the triangulation $\mathcal{T}$ through a global lower bound of the minimal angle therein) such that the exact (resp. discrete) stress σ from (1) [resp. σ_h from (3)] with $g - g_h \perp P_0(\mathcal{E}(\Gamma_N); \mathbb{R}^2)$ and the error estimator (4) satisfy*

$$\|\sigma - \sigma_h\|_{L^2(\Omega)} \le C_{rel}\eta(\mathcal{T}, \sigma_h).$$

The a posteriori error estimator $\eta(\mathcal{T}, \sigma_h)$ already involves two data oscillation terms $\operatorname{osc}(f,\mathcal{T})$ and $\operatorname{osc}(g - g_h, \mathcal{E}(\Gamma_N))$ defined as the square roots of the respective terms in

$$\operatorname{osc}^2(f,\mathcal{T}) := \sum_{T\in\mathcal{T}} h_T^2 \|f - f_h\|_{L^2(T)}^2 \text{ for the } L^2 \text{ projection } f_h \text{ of } f \text{ onto } P_k(\mathcal{T}; \mathbb{R}^2);$$

$$\operatorname{osc}^2(g - g_h, \mathcal{E}(\Gamma_N)) := \sum_{E\in\mathcal{E}(\Gamma_N)} h_E \|g - g_h\|_{L^2(E)}^2.$$

For any edge E and a degree $m \ge k+2$, let $\Pi_{m,E} : L^2(E) \to P_m(E)$ denote the L^2 projection onto polynomials of degree at most m. For any $E \in \mathcal{E}(\Gamma_D)$ define the two Dirichlet data oscillation terms

$$\operatorname{osc}_I^2(u_D, E) := h_E \|(1 - \Pi_{m,E})\partial(u_D \cdot \tau_E)/\partial s\|_{L^2(E)}^2, \tag{5}$$

$$\operatorname{osc}_{II}^2(u_D, E) := h_E^3 \|(1 - \Pi_{m,E})\partial^2(u_D \cdot \nu_E)/\partial s^2\|_{L^2(E)}^2. \tag{6}$$

Their sum defines the overall Dirichlet data approximation $\operatorname{osc}(u_D, \mathcal{E}(\Gamma_D))$ as the square root of

$$\operatorname{osc}^2(u_D, \mathcal{E}(\Gamma_D)) := \sum_{E\in\mathcal{E}(\Gamma_D)} \left(\operatorname{osc}_I^2(u_D, E) + \operatorname{osc}_{II}^2(u_D, E)\right).$$

The analysis of Sect. 3 is local and states for each of the five local residuals an upper bound related to the error in a neighborhood. The global efficiency is displayed as follows.

Theorem 2 (efficiency) *There exists a mesh-size and λ, μ independent constant C_{eff} (which may depend on the shape-regularity of the triangulation $\mathcal{T}$ through a global lower bound of the minimal angle therein) such that the exact (resp. discrete) stress σ from (1) [resp. σ_h from (3)] with $g - g_h \perp P_0(\mathcal{E}(\Gamma_N); \mathbb{R}^2)$ and the error estimator (4) satisfy*

$$C_{eff}^{-1}\eta(\mathcal{T}, \sigma_h) \le \|\sigma - \sigma_h\|_{L^2(\Omega)} + \mathrm{osc}(f, \mathcal{T}) + \mathrm{osc}(g - g_h, \mathcal{E}(\Gamma_N)) + \mathrm{osc}(u_D, \mathcal{E}(\Gamma_D)).$$

1.5 Outline of the paper

The remaining parts of this paper provide a mathematical proof of Theorems 1 and 2 and numerical evidence in computational experiments on the novel a posteriori error estimation and its robustness as well as on associated mesh-refining algorithms.

The proof of the reliability of Theorem 1 in Sect. 2 adopts arguments of [11,15] and carries out two integration by parts on each triangle plus one-dimensional integration by parts along all edges. The resulting terms are in fact locally efficient in Sect. 3 with little generalizations of the bubble-function methodology due to Verfürth [24]. The five lemmas of Sect. 3 give slightly sharper results and in total imply Theorem 2.

The point in Theorems 1 and 2 is that the universal constants C_{rel} and C_{eff} may depend on the Lamé parameter μ but are independent of the critical Lamé parameter λ as supported by the benchmark examples of the concluding Sect. 4. Adaptive mesh-refining proves to be highly effective with the novel a posteriori error estimator even for incompatible Neumann data. Four benchmark examples with the Poisson ratio $\nu = 0.3$ or 0.4999 provide numerical evidence of the robustness of the reliable and efficient a posteriori error estimation and for the fourth-order convergence of Theorem 5.

Three appendices highlight some improvements in the numerical benchmarks: Appendix A explains the improved convergence order for piecewise affine data and B and C explain how to treat incompatible Neumann data successfully.

1.6 Comments on general notation

Standard notation on Lebesgue and Sobolev spaces and norms is adopted throughout this paper and, for brevity, $\| \cdot \| := \| \cdot \|_{L^2(\Omega)}$ denotes the L^2 norm. The piecewise action of a differential operator is denoted with a subindex NC, e.g., ∇_{NC} denotes the piecewise gradient $(\nabla_{NC}\bullet)|_T := \nabla(\bullet|_T)$ for all $T \in \mathcal{T}$. Sobolev functions are usually defined on open sets and the notation $W^{m,p}(T)$ (resp. $W^{m,p}(\mathcal{T})$) substitutes $W^{m,p}(\mathrm{int}(T))$ for a (compact) triangle T and its interior $\mathrm{int}(T)$ (resp. $W^{m,p}(\mathrm{int}(\mathcal{T}))$) and their vector and matrix versions.

For a differentiable function ϕ, $\mathrm{Curl}\,\phi := (-\partial_2\phi, \partial_1\phi)$ is the rotated gradient; for a two-dimensional vector field Φ, $\mathrm{Curl}\,\Phi$ is the 2×2 matrix-valued rotated gradient

$$\operatorname{Curl} \Phi := (-\partial_2 \Phi_1, \partial_1 \Phi_1; -\partial_2 \Phi_2, \partial_1 \Phi_2) = D\Phi(0, 1; -1, 0).$$

(The signs are not uniquely determined in the literature and some care is required.)

The colon denotes the scalar product $A : B := \sum_{\alpha,\beta=1,2} A_{\alpha,\beta} B_{\alpha,\beta}$ of 2×2 matrices A, B. The inequality $A \lesssim B$ between two terms A and B abbreviates $A \leq C B$ with some multiplicative generic constant C, which is independent of the mesh-size and independent of the one Lamé parameter $\lambda \geq 0$ but may depend on the other $\mu > 0$ and may depend on the shape-regularity of the underlying triangulation $\mathscr{T}$ and the parameter k related to the polynomial degree of the scheme.

2 Proof of reliability

This section is devoted to the proof of Theorem 1 based on a Helmholtz decomposition of [11] with two parts as decomposed in Theorem 3 below. The critical part is the L^2 product of $\mathbb{C}^{-1}(\sigma - \sigma_h)$ times the Curl of an unknown function Curl β. The observation from [15] is that one can find an Argyris finite element approximation β_h to $\beta \in H^2(\Omega)$ such that the continuous function $\phi := \beta - \beta_h \in H^2(\Omega)$ vanishes at all vertices $\mathscr{N}$ of the triangulation. Two integration by parts on each triangle plus one-dimensional integration by parts along the edges $\mathscr{E}$ of the triangulation eventually lead to a key identity.

Lemma 1 (representation formula) *Any function $\boldsymbol{\varepsilon}_h \in H^2(\mathscr{T}; \mathbb{S})$ (i.e. $\boldsymbol{\varepsilon}_h$ is piecewise in H^2 with values in $\mathbb{S}$) and any $\phi \in H^2(\Omega)$ with $\phi(z) = 0$ at all vertices $z \in \mathscr{N}$ in the regular triangulation $\mathscr{T}$ satisfy*

$$(\boldsymbol{\varepsilon}_h, \operatorname{Curl}^2 \phi)_{L^2(\Omega)} = (\operatorname{rot}_{NC} \operatorname{rot}_{NC} \boldsymbol{\varepsilon}_h, \phi)_{L^2(\Omega)}$$
$$+ \sum_{E \in \mathscr{E}(\Omega)} \left((\tau_E \cdot [\boldsymbol{\varepsilon}_h]_E \tau_E, \partial_{\nu_E} \phi)_{L^2(E)} - \left([\operatorname{rot}_{NC} \boldsymbol{\varepsilon}_h]_E - \frac{\partial [\boldsymbol{\varepsilon}_h]_E \nu_E}{\partial s}, \phi \tau_E \right)_{L^2(E)} \right)$$
$$+ \sum_{E \in \mathscr{E}(\partial\Omega)} \left((\tau_E \cdot \boldsymbol{\varepsilon}_h \tau_E, \partial_{\nu_E} \phi)_{L^2(E)} - \left(\operatorname{rot} \boldsymbol{\varepsilon}_h - \frac{\partial \boldsymbol{\varepsilon}_h \nu_E}{\partial s}, \phi \tau_E \right)_{L^2(E)} \right).$$

The subsequent integration by parts formula is utilized frequently throughout this paper for $\phi \in H^1(\Omega; \mathbb{R}^2)$ and $\Psi \in H^1(\Omega; \mathbb{R}^{2 \times 2})$

$$\int_\Omega \Psi : \operatorname{Curl} \phi \, dx + \int_\Omega \phi \cdot \operatorname{rot} \Psi \, dx = \int_{\partial\Omega} \phi \cdot \Psi \tau_E \, ds.$$

Any differentiable (scalar) function φ, satisfies the elementary relations

$$\tau_E \cdot \operatorname{Curl} \varphi = \partial\varphi/\partial\nu_E \quad \text{and} \quad \nu_E \cdot \operatorname{Curl} \varphi = -\partial\varphi/\partial s = -\partial\varphi/\partial\tau_E \quad \text{on } E \in \mathscr{E}.$$

Proof Integrate by parts twice on each triangle and rearrange the remaining boundary terms to deduce (with the abbreviation $\operatorname{rot}_{NC} \operatorname{rot}_{NC} \equiv \operatorname{rot}^2_{NC}$)

$$(\boldsymbol{\varepsilon}_h, \operatorname{Curl}^2 \phi)_{L^2(\Omega)} = (\operatorname{rot}^2_{NC} \boldsymbol{\varepsilon}_h, \phi)_{L^2(\Omega)}$$
$$+ \sum_{E \in \mathscr{E}(\Omega)} \left(([\boldsymbol{\varepsilon}_h]_E \tau_E, \operatorname{Curl} \phi)_{L^2(E)} - ([\operatorname{rot}_{NC} \boldsymbol{\varepsilon}_h]_E \cdot \tau_E, \phi)_{L^2(E)} \right)$$
$$+ \sum_{E \in \mathscr{E}(\partial\Omega)} \left((\boldsymbol{\varepsilon}_h \tau_E, \operatorname{Curl} \phi)_{L^2(E)} - (\operatorname{rot} \boldsymbol{\varepsilon}_h \cdot \tau_E, \phi)_{L^2(E)} \right).$$

The term $([\boldsymbol{\varepsilon}_h]_E \tau_E, \operatorname{Curl} \phi)_{L^2(E)}$ in the above sum is split into orthogonal components

$$\operatorname{Curl} \phi = (\tau_E \cdot \operatorname{Curl} \phi)\tau_E + (\nu_E \cdot \operatorname{Curl} \phi)\nu_E$$
$$= (\tau_E \cdot \operatorname{Curl} \phi)\tau_E - (\partial \phi / \partial s)\nu_E \quad \text{on } E \in \mathscr{E}.$$

Since ϕ vanishes at the vertices, an integration by parts along each interior edge E for the last term shows $([\boldsymbol{\varepsilon}_h]_E \tau_E, (\partial \phi / \partial s)\nu_E)_{L^2(E)} = -(\partial [\boldsymbol{\varepsilon}_h]_E \tau_E / \partial s, \phi \nu_E)_{L^2(E)}$. This proves

$$([\boldsymbol{\varepsilon}_h]_E \tau_E, \operatorname{Curl} \phi)_{L^2(E)} = (\tau_E \cdot [\boldsymbol{\varepsilon}_h]_E \tau_E, \partial_{\nu_E} \phi)_{L^2(E)} + \left(\frac{\partial \nu_E \cdot [\boldsymbol{\varepsilon}_h]_E \tau_E}{\partial s}, \phi \right)_{L^2(E)}.$$

The same formula holds for any boundary edge E when $[\boldsymbol{\varepsilon}_h]_E$ is replaced by $\boldsymbol{\varepsilon}_h$. The combination of the latter identities with the first displayed formula of this proof verifies the asserted representation formula. □

The contribution of $\varepsilon(u) = \mathbb{C}^{-1}\sigma$ times the $\operatorname{Curl}^2 \phi \in L^2(\Omega; \mathbb{S})$ exclusively leads to boundary terms. Throughout this paper, suppose that the Dirichlet data u_D satisfies $u_D \in C(\Gamma_D) \cap H^2(\mathscr{E}(\Gamma_D))$ in the sense that u_D is globally continuous with $u_D|_E \in H^2(E; \mathbb{R}^2)$ for all $E \in \mathscr{E}(\Gamma_D)$.

Lemma 2 (boundary terms) *Any Sobolev function $v \in H^1(\Omega; \mathbb{R}^2)$ with boundary values $u_D \in C(\Gamma_D) \cap H^2(\mathscr{E}(\Gamma_D))$ on Γ_D and any $\phi \in H^2(\Omega)$ with $\phi = \partial \phi / \partial \nu = 0$ along Γ_N with $\phi(z) = 0$ for any vertex z of Γ_D in its relative interior satisfy*

$$(\varepsilon(v), \operatorname{Curl}^2 \phi)_{L^2(\Omega)} = \sum_{E \in \mathscr{E}(\Gamma_D)} \left(\left(\frac{\partial u_D}{\partial s}, \frac{\partial \phi}{\partial \nu_E} \tau_E \right)_{L^2(E)} + \left(\frac{\partial^2 u_D}{\partial s^2}, \phi \nu_E \right)_{L^2(E)} \right).$$

Proof A density argument shows that it suffices to prove this identity for smooth functions v and ϕ, when integration by parts arguments show that the left-hand side is equal to

$$\int_{\partial\Omega} \operatorname{Curl} \phi \cdot \frac{\partial v}{\partial s} ds = \sum_{E \in \mathscr{E}(\partial\Omega)} \int_E \left(\frac{\partial \phi}{\partial \nu_E} \frac{\partial(v \cdot \tau_E)}{\partial s} + \phi \frac{\partial^2 (v \cdot \nu_E)}{\partial s^2} \right) ds.$$

The equality follows from an orthogonal split $\operatorname{Curl} \phi = (\tau \cdot \operatorname{Curl} \phi)\tau + (\nu \cdot \operatorname{Curl} \phi)\nu$ into the normal and tangential directions of ν and τ along the boundary $\partial\Omega$ followed by an integration by parts along $\partial\Omega$ with $\phi(z) = 0$ for vertices z in Γ_D with a jump

of the normal unit vector. The substitution of the boundary conditions concludes the proof. □

The consequence of the previous two lemmas is a representation formula for the error times a typical function $\mathrm{Curl}^2 \phi$. To understand why the contributions on the Neumann boundary of ϕ and $\nabla \phi$ disappear along Γ_N, some details on the Helmholtz decomposition are recalled from the literature. For this, let $\Gamma_0, \ldots, \Gamma_J$ denote the compact connectivity components of $\overline{\Gamma_N}$.

Theorem 3 (Helmholtz decomposition [11, Lemma 3.2]) *For $\sigma - \sigma_h \in L^2(\Omega; \mathbb{S})$, there exists $\alpha \in V$, constant vectors $c_0, \ldots, c_J \in \mathbb{R}^2$ with $c_0 = 0$ and $\beta \in H^2(\Omega)$ with $\int_\Omega \beta\, dx = 0$ and $\mathrm{Curl}\, \beta = c_j$ on $\Gamma_j \subseteq \Gamma_N$ for all $j = 0, \ldots, J$ such that*

$$\sigma - \sigma_h = \mathbb{C}\varepsilon(\alpha) + \mathrm{Curl}\, \mathrm{Curl}\, \beta. \tag{7}$$

□

The second ingredient is an approximation β_h of β from the Helmholtz decomposition in Theorem 3 based on the Argyris finite element functions $A(\mathscr{T}) \subset C^1(\Omega) \cap P_5(\mathscr{T})$ [7,8,20]. The local mesh-size $h_{\mathscr{T}} \in P_0(\mathscr{T})$ in the triangulation $\mathscr{T}$ is defined as its diameter $h_{\mathscr{T}}|_T := h_T$ on each triangle $T \in \mathscr{T}$.

Lemma 3 (quasi-interpolation) *Given any β as in Theorem 3 there exists some $\beta_h \in A(\mathscr{T})$ such that $\phi := \beta - \beta_h \in H^2(\Omega)$ vanishes at any vertex $z \in \mathscr{N}$ of the triangulation, ϕ and its normal gradient $\nabla \phi \cdot \nu$ vanish on Γ_N, and the local approximation and stability property holds in the sense that*

$$\|h_{\mathscr{T}}^{-2}\phi\| + \|h_{\mathscr{T}}^{-1}\, \mathrm{Curl}\, \phi\| + \|\mathrm{Curl}^2\, \phi\| \lesssim \|\beta\|_{H^2(\Omega)}.$$

Proof This has been (partly) utilized in [15] and also follows from [21]. □

The combination of all aforementioned arguments leads to the following estimate as an answer to the question of Sect. 1.1 in terms of directional derivatives of $\varepsilon_h := \mathbb{C}^{-1}\sigma_h$. Recall the definition of $\eta(\mathscr{T}, \sigma_h)$ from (4).

Theorem 4 (key result) *Let $\sigma \in H(\mathrm{div}, \Omega; \mathbb{S})$ solve (1) and let $\sigma_h \in AW_k(\mathscr{T})$ solve (3). Given β from Theorem 3 and its quasi-interpolation β_h from Lemma 3, the difference $\phi := \beta - \beta_h$ satisfies*

$$(\mathbb{C}^{-1}(\sigma - \sigma_h), \mathrm{Curl}^2\, \phi)_{L^2(\Omega)} \lesssim |\beta|_{H^2(\Omega)}\eta(\mathscr{T}, \sigma_h).$$

Proof Lemmas 1 and 2 lead to a formula for $(\varepsilon_h, \mathrm{Curl}^2\, \phi)_{L^2(\Omega)}$, $\varepsilon_h := \mathbb{C}^{-1}\sigma_h$, in which all the contributions for $E \in \mathscr{E}(\Gamma_N)$ with ϕ and $\nabla \phi$ vanish along Γ_N. The remaining formula reads

$$(\mathbb{C}^{-1}(\sigma - \sigma_h), \operatorname{Curl}^2 \phi)_{L^2(\Omega)} = -(\operatorname{rot}_{NC}^2 \boldsymbol{\varepsilon}_h, \phi)_{L^2(\Omega)}$$

$$- \sum_{E \in \mathscr{E}(\Omega)} \left(\left(\tau_E \cdot [\boldsymbol{\varepsilon}_h]_E \tau_E, \frac{\partial \phi}{\partial \nu_E} \right)_{L^2(E)} - \left([\operatorname{rot}_{NC} \boldsymbol{\varepsilon}_h]_E - \frac{\partial [\boldsymbol{\varepsilon}_h]_E \nu_E}{\partial s}, \phi \tau_E \right)_{L^2(E)} \right)$$

$$+ \sum_{E \in \mathscr{E}(\Gamma_D)} \left(\left(\frac{\partial u_D}{\partial s} - \boldsymbol{\varepsilon}_h \tau_E, \tau_E \frac{\partial \phi}{\nu_E} \right)_{L^2(E)} \right.$$

$$+ \left. \left(\tau_E \cdot \left(\operatorname{rot}_{NC} \boldsymbol{\varepsilon}_h - \frac{\partial (\boldsymbol{\varepsilon}_h \nu_E)}{\partial s} \right) + \frac{\partial^2 u_D \cdot \nu_E}{\partial s^2}, \phi \right)_{L^2(E)} \right).$$

The proof concludes with Cauchy–Schwarz inequalities, trace inequalities, and the approximation estimates of Lemma 3. The remaining details are nowadays standard arguments in the a posteriori error analysis of nonconforming and mixed finite element methods and hence are omitted. □

Before the proof of Theorem 1 concludes this section, three remarks and one lemma are in order.

Remark 1 *(nonconstant coefficients)* The main parts of the reliability analysis of this section hold for rather general material tensors $\mathbb{C}$ as long as $\boldsymbol{\varepsilon}_h := \mathbb{C}^{-1}\sigma_h$ allows for the existence of the traces and the derivatives in the error estimator (4) in the respective L^2 spaces. For instance, if λ and μ are piecewise smooth with respect to the underlying triangulation $\mathscr{T}$.

Remark 2 *(constant coefficients)* The overall assumption of constant Lamé parameters λ and μ allows a simplification in the error estimator (4). It suffices to have μ globally continuous and μ and λ piecewise smooth to guarantee

$$\frac{\partial [\boldsymbol{\varepsilon}_h]_E \nu_E}{\partial s} \cdot \tau_E = 0 \quad \text{along } E \in \mathscr{E}(\Omega).$$

(The proof utilizes the structure of $\mathbb{C}^{-1}$ with $\mathbb{C}^{-1}E = \frac{1}{2\mu}(E - \frac{\lambda}{2(\lambda+\mu)} \operatorname{tr}(E)1_{2\times 2})$ for any $E \in \mathbb{S}$ as a linear combination of the identity and some scalar multiple of the 2×2 unit matrix. The terms with the identity lead to $1/(2\mu)$ times the jump $[\sigma_h]_E \nu_E = 0$ of the $H(\operatorname{div})$ conforming stress approximations. The jump terms with the unit matrix (even with jumps of λ) are multiplied with the orthogonal unit vectors ν_E and τ_E and so vanish as well.)

Remark 3 *(related work)* Although the work [22] concerns a different problem (bending of a plate of fourth order) with a different discretization (even nonconforming in $H(\operatorname{div})$), some technical parts of that paper are related to those of this by a rotation of the underlying coordinate system and the substitution of div div by rot rot etc. Another Helmholtz decomposition also allows for a discrete version and thereby enables a proof of optimal convergence of an adaptive algorithm with arguments from [13,19].

A technical detail related to the robustness in $\lambda \to \infty$ is a well known lemma that controls the trace of a matrix $E \in \mathbb{R}^{2\times 2}$ by its deviatoric part $\operatorname{dev} E := E - \operatorname{tr}(E)/2\ 1_{2\times 2}$ and its divergence measured in the dual $V^* \subset H^{-1}(\Omega; \mathbb{R}^2)$ of V, namely

$$\| \operatorname{div} \tau \|_{-1} := \sup_{\substack{v \in V \\ |v|_{H^1(\Omega)}=1}} \int_{\Omega} \tau : Dv \, dx \quad \text{for all } \tau \in L^2(\Omega; \mathbb{R}^{2 \times 2}).$$

Lemma 4 (tr-dev-div) *Let Σ_0 be a closed subspace of $H(\operatorname{div}, \Omega; \mathbb{R}^{2 \times 2})$, which does not contain the constant tensor $1_{2 \times 2}$. Then any $\tau \in \Sigma_0$ satisfies*

$$\| \operatorname{tr}(\tau) \|_{L^2(\Omega)} \lesssim \| \operatorname{dev} \tau \|_{L^2(\Omega)} + \| \operatorname{div} \tau \|_{-1}.$$

Proof There are several variants of the tr-dev-div lemma known in the literature [6, Proposition 9.1.1]. The version in [11, Theorem 4.1] explicitly displays a version with $\| \operatorname{div} \tau \|$ replacing $\| \operatorname{div} \tau \|_{-1}$. Since its proof is immediately adopted to prove the asserted version, further details are omitted. □

The remaining part of this section outlines why Theorem 1 follows from Theorem 4 with the arguments from [11,15]. The energy norms for any $v \in V$ and $\tau \in H(\operatorname{div}, \Omega; \mathbb{S})$ read

$$\|v\|^2 := \int_{\Omega} \varepsilon(v) : \mathbb{C}\varepsilon(v) \, dx \quad \text{and} \quad \|\tau\|_{\mathbb{C}^{-1}}^2 := \int_{\Omega} \tau : \mathbb{C}^{-1}\tau \, dx.$$

The remaining residual is denoted by

$$\operatorname{Res}(v) := \int_{\Omega} f \cdot v \, dx + \int_{\Gamma_N} g \cdot v \, ds - \int_{\Omega} \sigma_h : \varepsilon(v) \, dx \quad \text{for all } v \in V$$

with its dual norm

$$\|\operatorname{Res}\|_* := \sup_{\substack{v \in V \\ \|v\|=1}} \operatorname{Res}(v).$$

It is shown in the proof of [15, Theorem 3.1] that $\alpha \in V$ and $\beta \in H^2(\Omega)$ from the Helmholtz decomposition of the error $\sigma - \sigma_h$ in Theorem 3 are orthogonal with respect to the L^2 scalar product weighted with $\mathbb{C}^{-1}$. This implies

$$\|\sigma - \sigma_h\|_{\mathbb{C}^{-1}}^2 = (\sigma - \sigma_h, \varepsilon(\alpha))_{L^2(\Omega)} + (\mathbb{C}^{-1}(\sigma - \sigma_h), \operatorname{Curl}^2 \beta)_{L^2(\Omega)}. \quad (8)$$

Let β_h denote the quasi-interpolation of β from Lemma 3. It is known [15] that $\operatorname{Curl}^2 \beta_h$ is a divergence-free element of $\Sigma(0, \mathscr{T})$. Therefore, (2) and (3) imply

$$(\mathbb{C}^{-1}(\sigma - \sigma_h), \operatorname{Curl}^2 \beta_h)_{L^2(\Omega)} = 0.$$

Thus, with $\phi = \beta - \beta_h$, the second term of (8) equals $(\mathbb{C}^{-1}(\sigma - \sigma_h), \operatorname{Curl}^2 \phi)_{L^2(\Omega)}$ and hence is controlled in the key estimate of Theorem 4 as

$$(\mathbb{C}^{-1}(\sigma - \sigma_h), \operatorname{Curl}^2 \beta)_{L^2(\Omega)} \lesssim |\beta|_{H^2(\Omega)} \eta(\mathscr{T}, \sigma_h).$$

Lemma 4 applies to Σ_0 as the subspace of all $\tau \in H(\mathrm{div}, \Omega; \mathbb{S})$ with homogeneous Neumann data $\tau \nu = 0$ along Γ_N. Since $\tau := \mathrm{Curl}^2 \beta$ is divergence free (by the relation $\mathrm{div}\, \mathrm{Curl} = 0$) and since $\tau \nu = -\partial \, \mathrm{Curl}\, \beta / \partial s$ along Γ_N (owing to the aforementioned elementary relations and the convention that the first Curl acts row-wise on $\mathrm{Curl}\, \beta$), where $\mathrm{Curl}\, \beta$ in Theorem 3 is piecewise constant, it follows that $\tau \in \Sigma_0$. On the other hand $1_{2 \times 2} \notin \Sigma_0$ because $\Gamma_N \neq \emptyset$. Consequently, Lemma 4 implies $\| \mathrm{Curl}^2 \beta \| \lesssim \| \mathrm{dev}\, \mathrm{Curl}^2 \beta \|$. This and elementary calculations with $\mathbb{C}^{-1}$ lead to

$$|\beta|_{H^2(\Omega)} = \| \mathrm{Curl}^2 \beta \| \lesssim \| \mathrm{dev}\, \mathrm{Curl}^2 \beta \| \lesssim \| \mathrm{Curl}^2 \beta \|_{\mathbb{C}^{-1}}.$$

The combination with the estimate resulting from Theorem 4 proves

$$(\mathbb{C}^{-1}(\sigma - \sigma_h), \mathrm{Curl}^2 \beta)_{L^2(\Omega)} \lesssim \| \mathrm{Curl}^2 \beta \|_{\mathbb{C}^{-1}} \, \eta(\mathscr{T}, \sigma_h).$$

This, the stability $\| \mathrm{Curl}^2 \beta \|_{\mathbb{C}^{-1}} \leq \| \sigma - \sigma_h \|_{\mathbb{C}^{-1}}$, and $\|\alpha\| = \|\mathrm{Res}\|_*$ lead in (8) to

$$\| \sigma - \sigma_h \|_{\mathbb{C}^{-1}} \lesssim \|\mathrm{Res}\|_* + \eta(\mathscr{T}, \sigma_h). \tag{9}$$

The remaining term is the estimate of the dual norm $\|\mathrm{Res}\|_*$ of the residual which is done, e.g., in [15, Lemma 3.3] (under the assumption $g - g_h \perp P_0(\mathscr{E}(\Gamma_N))$)

$$\|\mathrm{Res}\|_* \lesssim \mathrm{osc}(f, \mathscr{T}) + \mathrm{osc}(g - g_h, \mathscr{E}(\Gamma_N)) \leq \eta(\mathscr{T}, \sigma_h).$$

This and (9) imply

$$\| \mathrm{dev}(\sigma - \sigma_h) \| \lesssim \| \sigma - \sigma_h \|_{\mathbb{C}^{-1}} \lesssim \eta(\mathscr{T}, \sigma_h).$$

For any test function $v \in V$ with $|v|_{H^1(\Omega)} = 1$, $\int_\Omega (\sigma - \sigma_h) : Dv \, dx = \mathrm{Res}(v)$ and so

$$\| \mathrm{div}(\sigma - \sigma_h) \|_{-1} = \sup_{\substack{v \in V \\ |v|_{H^1(\Omega)} = 1}} \mathrm{Res}(v) \leq \sup_{\substack{v \in V \\ \|\varepsilon(v)\| = 1}} \mathrm{Res}(v) \leq 2\mu \, \|\mathrm{Res}\|_* \lesssim \eta(\mathscr{T}, \sigma_h).$$

(In the second last step one utilizes that $2\mu \, E : E \leq E : \mathbb{C}E$ for all $E \in \mathbb{S}$.) The combination of Lemma 4 for $\tau = \sigma - \sigma_h$ with the previous displayed estimates concludes the proof of $\| \sigma - \sigma_h \| \lesssim \eta(\mathscr{T}, \sigma_h)$. There exist several appropriate choices of $\Sigma_0 \subset H(\mathrm{div}, \Omega; \mathbb{S})$ in this last step. Recall that Γ_N is the union of connectivity components and so pick one edge E_0 in this polygon and consider $\Sigma_0 := \{\tau \in H(\mathrm{div}, \Omega; \mathbb{S}) : \int_{E_0} \tau \nu \, ds = 0\}$ with $1_{2 \times 2} \notin \Sigma_0$. This choice of E_0 and so Σ_0 depend only on Γ_N (independent of $\mathscr{T}$). Since $g - g_h = (\sigma - \sigma_h)\nu$ along E_0 has (piecewise on $\mathscr{E}(E_0)$, whence in total) an integral mean zero, Lemma 4 indeed applies to $\tau = \sigma - \sigma_h \in \Sigma_0$. $\qquad\square$

3 Local efficiency analysis

The local efficiency follows with the bubble-function technique for C^1 finite elements [24, Sec 3.7]. This section focuses on a constant $\mathbb{C}$ for linear isotropic elasticity with constant Lamé parameters λ and μ such that $\boldsymbol{\varepsilon}_h := \mathbb{C}^{-1}\sigma_h \in P_{k+2}(\mathscr{T})$ for some $\sigma_h \in AW_k(\mathscr{T})$ is a polynomial of degree at most $k+2$. Apart from this, the Lamé parameters do not further arise in this section.

The moderate point of departure is the volume term for each triangle $T \in \mathscr{T}$ with barycentric coordinates $\lambda_1, \lambda_2, \lambda_3 \in P_1(T)$ and their product, the cubic volume bubble function, $b_T := 27\,\lambda_1\lambda_2\lambda_3 \in W_0^{1,\infty}(T)$ plus its square $b_T^2 \in W_0^{2,\infty}(T)$ with $0 \le b_T^2 \le 1$, $\|b_T\|_{L^2(T)} \lesssim 1$, and $|b_T|_{H^2(T)} \lesssim h_T^{-2}$ etc.

Lemma 5 (efficiency of volume residual) *Any $v \in H^1(T; \mathbb{R}^2)$, $T \in \mathscr{T}$, satisfies*

$$h_T^2\|\operatorname{rot}\operatorname{rot}\boldsymbol{\varepsilon}_h\|_{L^2(T)} \lesssim \|\boldsymbol{\varepsilon}_h - \varepsilon(v)\|_{L^2(T)}.$$

Proof An inverse estimate for the polynomial $\operatorname{rot}\operatorname{rot}\boldsymbol{\varepsilon}_h \equiv \operatorname{rot}^2 \boldsymbol{\varepsilon}_h$ implies the estimate

$$\|\operatorname{rot}^2\boldsymbol{\varepsilon}_h\|_{L^2(T)}^2 \lesssim \|b_T\operatorname{rot}^2\boldsymbol{\varepsilon}_h\|_{L^2(T)}^2 = (\operatorname{rot}^2\boldsymbol{\varepsilon}_h, b_T^2\operatorname{rot}^2\boldsymbol{\varepsilon}_h)_{L^2(T)}.$$

Lemma 1 with $\phi = b_T^2\operatorname{rot}^2\boldsymbol{\varepsilon}_h$ and $(\varepsilon(v), \operatorname{Curl}^2\phi)_{L^2(T)} = 0$ leads to

$$\|b_T\operatorname{rot}^2\boldsymbol{\varepsilon}_h\|_{L^2(T)}^2 = (\boldsymbol{\varepsilon}_h - \varepsilon(v), \operatorname{Curl}^2(b_T^2\operatorname{rot}^2\boldsymbol{\varepsilon}_h))_{L^2(T)}$$
$$\le \|\boldsymbol{\varepsilon}_h - \varepsilon(v)\|_{L^2(T)}\|\operatorname{Curl}^2(b_T^2\operatorname{rot}^2\boldsymbol{\varepsilon}_h)\|_{L^2(T)}.$$

This and the inverse estimate $\|\operatorname{Curl}^2(b_T^2\operatorname{rot}^2\boldsymbol{\varepsilon}_h)\|_{L^2(T)} \lesssim h_T^{-2}\|b_T^2\operatorname{rot}^2\boldsymbol{\varepsilon}_h\|_{L^2(T)}$ imply

$$\|\operatorname{rot}^2\boldsymbol{\varepsilon}_h\|_{L^2(T)}^2 \lesssim \|\boldsymbol{\varepsilon}_h - \varepsilon(v)\|_{L^2(T)}h_T^{-2}\|\operatorname{rot}^2\boldsymbol{\varepsilon}_h\|_{L^2(T)}.$$

This concludes the proof. □

The localization of the first edge residual involves the piecewise quadratic edge-bubble function b_E with support $T_+ \cup T_-$ for an interior edge $E = \partial T_+ \cap \partial T_-$ shared by the two triangles T_+ and T_- with edge-patch $\omega_E := (T_+\cup T_-)$. With an appropriate scaling $b_E|_T = 4\lambda_1\lambda_2$ for the two barycentric coordinates λ_1, λ_2 on $T \in \{T_+, T_-\}$ associated with the two vertices of E. Then $b_E \in W^{1,\infty}(\omega_E)$ and $b_E^2 \in W^{2,\infty}(\omega_E)$ satisfy $0 \le b_E^2 \le b_E \le 1$ and $|b_E|_{H^1(E)} \lesssim h_E^{-1}$ etc.

The remaining technical detail is an extension of functions on the edge E to ω_E. Throughout this section those functions are polynomials and given $\rho_E \in P_m(E)$, their coefficients (in some fixed basis) already define an algebraic object that is a natural extension $\rho \in P_m(\hat{E})$ along the straight line $\hat{E} := \operatorname{mid}(E) + \mathbb{R}\,\tau_E$ that extends E with midpoint $\operatorname{mid}(E)$ and tangential unit vector τ_E. This and

$$P_E(\rho_E)(x) := \rho(\tau_E \cdot (x - \operatorname{mid}(E))) \quad \text{for all } x \in \mathbb{R}^2$$

define a linear extension operator $P_E : P_m(E) \to C^\infty(\mathbb{R}^2)$ with $P_E(\rho_E) = \rho_E$ on E for any $\rho_E \in P_m(E)$, which is constant in the normal direction, $\nabla P_E(\rho_E) \cdot \nu_E \equiv 0$. This design is different from that in [24].

Lemma 6 (efficiency of first interior edge residual) *Any* $v \in H^1(\omega_E; \mathbb{R}^2)$, $E \in \mathcal{E}(\Omega)$, *satisfies*

$$h_E^{1/2} \| \tau_E \cdot [\boldsymbol{\varepsilon}_h]_E \tau_E \|_{L^2(E)} \lesssim \| \boldsymbol{\varepsilon}_h - \varepsilon(v) \|_{L^2(\omega_E)}.$$

Proof Since $\tau_E \cdot [\boldsymbol{\varepsilon}_h]_E \tau_E \in P_{k+2}(E)$ is a polynomial, the above extension $P_E(\tau_E \cdot [\boldsymbol{\varepsilon}_h]_E \tau_E)$ and the function $b \in W_0^{2,\infty}(\omega_E)$ with

$$b(x) := b_E^2(x) \, \nu_E \cdot (x - \text{mid}(E)) \quad \text{for all } x \in \mathbb{R}^2 \tag{10}$$

define some function $\phi := b \, P_E(\tau_E \cdot [\boldsymbol{\varepsilon}_h]_E \tau_E)$. Since $b = 0$ and $\nabla b_E \cdot \nu_E = b_E^2$ along E, the test function $\phi \in H_0^2(\omega_E) \subset H_0^2(\Omega)$ leads in Lemma 1 to

$$(\tau_E \cdot [\boldsymbol{\varepsilon}_h]_E \tau_E, \partial_{\nu_E} \phi)_{L^2(E)} = (\boldsymbol{\varepsilon}_h, \text{Curl}^2 \phi)_{L^2(\omega_E)} - (\text{rot}_{NC}^2 \boldsymbol{\varepsilon}_h, \phi)_{L^2(\omega_E)}.$$

Since $\partial_{\nu_E} \phi = b_E^2 \, \tau_E \cdot [\boldsymbol{\varepsilon}_h]_E \tau_E$ on E and $\varepsilon(v) \perp \text{Curl}^2 \phi$, an inverse estimate shows

$$\| \tau_E \cdot [\boldsymbol{\varepsilon}_h]_E \tau_E \|_{L^2(E)}^2 \lesssim (\boldsymbol{\varepsilon}_h - \varepsilon(v), \text{Curl}^2 \phi)_{L^2(\omega_E)} - (\text{rot}_{NC}^2 \boldsymbol{\varepsilon}_h, \phi)_{L^2(\omega_E)}.$$

At the heart of the bubble-function methodology are inverse and trace inequalities that allow for appropriate scaling properties [24] under the overall assumption of shape-regularity. In the present case, one power of $h_E \approx h_{T_\pm}$ is hidden in the function b and

$$h_E^{1/2} |\phi|_{H^2(\omega_E)} + h_E^{-3/2} \|\phi\|_{L^2(\omega_E)} \lesssim \| \tau_E \cdot [\boldsymbol{\varepsilon}_h]_E \tau_E \|_{L^2(E)}. \tag{11}$$

The combination with the previous estimate results in

$$\| \tau_E \cdot [\boldsymbol{\varepsilon}_h]_E \tau_E \|_{L^2(E)}^2$$
$$\lesssim \| \tau_E \cdot [\boldsymbol{\varepsilon}_h]_E \tau_E \|_{L^2(E)} \left(h_E^{-1/2} \| \boldsymbol{\varepsilon}_h - \varepsilon(v) \|_{L^2(\omega_E)} + h_E^{3/2} \| \text{rot}_{NC}^2 \boldsymbol{\varepsilon}_h \|_{L^2(\omega_E)} \right).$$

This and Lemma 5 conclude the proof. $\qquad \square$

For any edge $E \in \mathcal{E}(\Gamma_D)$, the edge-bubble function $b_E = 4\lambda_1 \lambda_2 \in W^{1,\infty}(\omega_E)$ for the two barycentric coordinates λ_1, λ_2 associated with the two vertices of E and b_E vanishes on the remaining sides $\partial \omega_E \backslash E$ of the aligned triangle $\overline{\omega_E}$. The Dirichlet data u_D allows for some polynomial approximation $\Pi_{m,E} u_D \in P_m(E)$ of a maximal degree bounded by $m \geq k + 2$; recall the definition of $\text{osc}_I(u_D, E)$ from (5).

Lemma 7 (efficiency of first boundary edge residual) *Any* $v \in H^1(\omega_E; \mathbb{R}^2)$ *with* $v|_E = u_D|_E$ *along* $E \in \mathscr{E}(\Gamma_D)$ *satisfies*

$$h_E^{1/2} \|\tau_E \cdot (\boldsymbol{\varepsilon}_h \tau_E - \partial u_D/\partial s)\|_{L^2(E)} \lesssim \|\boldsymbol{\varepsilon}_h - \varepsilon(v)\|_{L^2(\omega_E)} + \mathrm{osc}_I(u_D, E).$$

Proof Since $\tau_E \cdot \boldsymbol{\varepsilon}_h \tau_E$ is a polynomial of degree at most $k + 2 \leq m$ along the exterior edge E, the residual $\tau_E \cdot (\boldsymbol{\varepsilon}_h \tau_E - \partial u_D/\partial s)$ is well approximated by its L^2 projection $\rho_E := (\tau_E \cdot (\boldsymbol{\varepsilon}_h \tau_E - \Pi_{m,E} \partial u_D/\partial s))$ onto $P_m(E)$. The Pythagoras theorem based on the L^2 orthogonality reads

$$h_E \|\tau_E \cdot (\boldsymbol{\varepsilon}_h \tau_E - \partial u_D/\partial s)\|_{L^2(E)}^2 = h_E \|\rho_E\|_{L^2(E)}^2 + \mathrm{osc}_I^2(u_D, E)$$

and it remains to bound $h_E^{1/2} \|\rho_E\|_{L^2(E)}$ by the right-hand side of the claimed inequality. The extension $P_E \rho_E \in C^\infty(\mathbb{R}^2)$ and the function b from (10) lead to an admissible test function $\phi := b P_E \rho_E \in W_0^{2,\infty}(\omega_E)$. Two successive integration by parts as in Lemma 1 show

$$(\varepsilon(v), \mathrm{Curl}^2 \phi)_{L^2(\omega_E)} = (\partial u_D/\partial s, \tau_E (\nu_E \cdot \nabla \phi))_{L^2(E)}.$$

This and Lemma 1 lead to

$$\left(\tau_E \cdot \left(\boldsymbol{\varepsilon}_h \tau_E - \frac{\partial u_D}{\partial s} \right), \frac{\partial \phi}{\partial \nu_E} \right)_{L^2(E)} = (\boldsymbol{\varepsilon}_h - \varepsilon(v), \mathrm{Curl}^2 \phi)_{L^2(\omega_E)} - (\mathrm{rot}_{NC}^2 \boldsymbol{\varepsilon}_h, \phi)_{L^2(\omega_E)}.$$

Since $\partial_{\nu_E} \phi = b_E^2 \rho_E$ along E and ρ_E is the L^2 projection of $\tau_E \cdot (\boldsymbol{\varepsilon}_h \tau_E - \partial u_D/\partial s)$, the left-hand side equals $\|b_E \rho_E\|_{L^2(E)}^2 - ((1 - \Pi_{m,E}) \partial u_D/\partial s, b_E^2 \rho_E)_{L^2(E)}$. The scaling argument which leads to (11) shows that the left-hand side of (11) is $\lesssim \|\rho_E\|_{L^2(E)}$. The combination with the previously displayed identity leads to

$$\|\rho_E\|_{L^2(E)}^2 \lesssim \|\rho_E\|_{L^2(E)} \Big(h_E^{-1/2} \|\boldsymbol{\varepsilon}_h - \varepsilon(v)\|_{L^2(\omega_E)}$$
$$+ h_E^{3/2} \|\mathrm{rot}_{NC}^2 \boldsymbol{\varepsilon}_h\|_{L^2(\omega_E)} + h_E^{-1/2} \mathrm{osc}_I(E, u_D) \Big).$$

This and Lemma 5 conclude the proof.   □

The edge-bubble functions for the second edge residuals are defined slightly differently to ensure some vanishing normal derivative.

Lemma 8 (efficiency of second interior edge residual) *Any* $v \in H^1(\omega_E; \mathbb{R}^2)$, $E \in \mathscr{E}(\Omega)$, *satisfies*

$$h_E^{3/2} \|\tau_E \cdot ([\mathrm{rot}_{NC} \boldsymbol{\varepsilon}_h]_E - \partial[\boldsymbol{\varepsilon}_h]_E/\partial s \, \nu_E)\|_{L^2(E)} \lesssim \|\boldsymbol{\varepsilon}_h - \varepsilon(v)\|_{L^2(\omega_E)}.$$

Proof There are many ways to define an edge-bubble function for this situation and one may first select a maximal open ball $B(x_E, 2r_E) \subset \omega_E$ around a point

$x_E \in E$ with maximal radius $2r_E$, which is entirely included in ω_E. The characteristic function $\chi_{B(x_E, r_E)}$ of the smaller ball $B(x_E, r_E)$ may be regularized with a standard mollification η_{r_E} to define the smooth function $b := \chi_{B(x_E, r_E)} * \eta_{r_E} \in C_c^\infty(\Omega_E)$ with values in $[0, 1]$ and with $\nabla b \cdot \nu_E = 0$ along E. The polynomial $\rho_E := \tau_E \cdot ([\mathrm{rot}_{NC} \, \boldsymbol{\varepsilon}_h]_E - \partial [\boldsymbol{\varepsilon}_h]_E / \partial s \, \nu_E)$ and its extension $P_E \rho_E$ define the test function $\phi := b P_E \rho_E \in C_0^\infty(\omega_E)$ in Lemma 1. The representation formula and $(\varepsilon(v), \mathrm{Curl}^2 \, \phi)_{L^2(\omega_E)} = 0$ lead to

$$\|b^{1/2} \rho_E\|_{L^2(E)}^2 = (\varepsilon(v) - \boldsymbol{\varepsilon}_h, \mathrm{Curl}^2 \, \phi)_{L^2(\omega_E)} + (\mathrm{rot}_{NC}^2 \, \boldsymbol{\varepsilon}_h, \phi)_{L^2(\omega_E)}.$$

The inverse inequality $\|\rho_E\|_{L^2(E)} \lesssim \|b^{1/2} \rho_E\|_{L^2(E)}$, Cauchy-Schwarz inequalities, and the right scaling properties of ϕ lead to

$$\|\rho_E\|_{L^2(E)}^2 \lesssim \|\rho_E\|_{L^2(E)} \left(h_E^{-3/2} \|\boldsymbol{\varepsilon}_h - \varepsilon(v)\|_{L^2(\omega_E)} + h_E^{1/2} \| \mathrm{rot}_{NC}^2 \, \boldsymbol{\varepsilon}_h \|_{L^2(\omega_E)} \right).$$

This and Lemma 5 conclude the proof.   □

The efficiency of the last edge contribution involves the second Dirichlet data oscillation $\mathrm{osc}_{II}(u_D, E)$ from (6).

Lemma 9 (efficiency of second boundary edge residual) *Any* $v \in H^1(\omega_E; \mathbb{R}^2)$ *with* $v|_E = u_D|_E$ *along* $E \in \mathscr{E}(\Gamma_D)$ *satisfies*

$$h_E^{3/2} \|\tau_E \cdot \mathrm{rot} \, \boldsymbol{\varepsilon}_h - \nu_E \cdot \left(\frac{\partial \boldsymbol{\varepsilon}_h \tau_E}{\partial s} - \frac{\partial^2 u_D}{\partial s^2} \right) \|_{L^2(E)}$$
$$\lesssim \|\boldsymbol{\varepsilon}_h - \varepsilon(v)\|_{L^2(\omega_E)} + \mathrm{osc}_{II}(u_D, E).$$

Proof Select a maximal open ball $B(x_E, 2r_E) \cap \Omega \subset \omega_E$ around a point $x_E \in E$ with maximal radius $2r_E$ such that $B(x_E, 2r_E) \cap \omega_E$ is a half ball. The regularization $b := \chi_{B(x_E, r_E)} * \eta_{r_E} \in C_c^\infty(\mathbb{R}^2)$ of the characteristic function $\chi_{B(x_E, r_E)}$ attains values in $[0, 1]$ and a positive integral mean $h_E^{-1} \int_E b \, ds \approx 1$ along E (depending only on the shape regularity of $\mathscr{T}$); b vanishes on $\partial \omega_E \backslash E$ and its normal derivative $\nabla b \cdot \nu = 0$ vanishes along the entire boundary $\partial \omega_E$.

The Pythagoras theorem $\|\rho\|_{L^2(E)}^2 = \|\rho_E\|_{L^2(E)}^2 + h_E^{-3} \, \mathrm{osc}_{II}^2(u_D, E)$ for the residual $\rho := \tau_E \cdot \mathrm{rot} \, \boldsymbol{\varepsilon}_h - \nu_E \cdot (\frac{\partial \boldsymbol{\varepsilon}_h \tau_E}{\partial s} - \frac{\partial^2 u_D}{\partial s^2})$ and its L^2 projection $\rho_E := \Pi_{m, E} \rho$ onto $P_m(E)$ reduces the proof to the estimation of $\|\rho_E\|_{L^2(E)}$. The normal derivative of $\phi := b \, P_E \rho_E \in C^\infty(\overline{\omega_E})$ vanishes along the boundary $\partial \omega_E$ and Lemma 1 shows

$$\left(\mathrm{rot} \, \boldsymbol{\varepsilon}_h - \frac{\partial \boldsymbol{\varepsilon}_h \nu_E}{\partial s}, b \rho_E \tau_E \right)_{L^2(E)} = (\mathrm{rot}_{NC}^2 \, \boldsymbol{\varepsilon}_h, \phi)_{L^2(\omega_E)} - (\boldsymbol{\varepsilon}_h, \mathrm{Curl}^2 \, \phi)_{L^2(\omega_E)}.$$

The arguments in Lemma 2 show $(\partial^2 u_D / \partial s^2, b \rho_E \, \nu_E)_{L^2(E)} = (\varepsilon(v), \mathrm{Curl}^2 \, \phi)_{L^2(\omega_E)}$. The combination of the two identities leads to a formula for $(\rho, b \rho_E)_{L^2(E)}$. Since $\rho - \rho_E$ is controlled in $\mathrm{osc}_{II}^2(u_D, E)$, this and an inverse inequality in the beginning result in

$$\|\rho_E\|^2_{L^2(E)} \lesssim (b\rho_E, \rho_E)_{L^2(E)} = (\rho, b\rho_E)_{L^2(E)} - (\rho - \rho_E, b\rho_E)_{L^2(E)}$$

$$\lesssim (\text{rot}^2_{NC}\, \boldsymbol{\varepsilon}_h, \phi)_{L^2(\omega_E)} - (\boldsymbol{\varepsilon}_h - \varepsilon(v), \text{Curl}^2\, \phi)_{L^2(\omega_E)} + \|\rho_E\|_{L^2(E)} h_E^{-3/2} \text{osc}_{II}(u_D, E).$$

The scaling properties of ϕ and its derivatives are as in the proof of the previous lemma. With Lemma 5 in the end, this concludes the proof.   □

4 Numerical examples

This section is devoted to numerical experiments for four different domains to demonstrate robustness in the reliability and efficiency of the a posteriori error estimator $\eta(\mathcal{T}_\ell, \sigma_\ell)$. The implementation follows [12,15,16] for $k = 1$ with Lamé parameters λ and μ from $\lambda = E\nu/((1+\nu)(1-2\nu))$ and $\mu = E/(2(1+\nu))$ for a Young's modulus $E = 10^5$ and various Poisson ratios $\nu = 0.3$ and $\nu = 0.4999$.

4.1 Academic example

The model problem (1) on the unit square $\Omega = (0, 1)^2$ with homogeneous Dirichlet boundary conditions and the right-hand side $f = (f_1, f_2)$,

$$f_1(x, y) = -f_2(y, x) = -2\mu\pi^3 \cos(\pi y) \sin(\pi y)(2 \cos(2\pi x) - 1) \quad \text{for } (x, y) \in \Omega,$$

allows the smooth exact solution

$$u(x, y) = \pi \sin(\pi x) \sin(\pi y) (\cos(\pi y) \sin(\pi x), - \cos(\pi x) \sin(\pi y)) \quad \text{for } (x, y) \in \Omega.$$

Note that f depends only on the Lamé parameter μ and not on the critical Lamé parameter λ. For uniform mesh refinement, Fig. 1 displays the robust third-order convergence of the a posteriori error estimator $\eta(\mathcal{T}_\ell, \sigma_\ell)$ as well as the Arnold–Winther finite element stress error. The convergence is robust in the Poisson ratio $\nu \to 1/2$ and the a posteriori error estimator proves to be reliable and efficient. In this example, the oscillations $\text{osc}(f, \mathcal{T}_\ell)$ dominate the a posteriori error estimator.

This typical observation motivates numerical examples with $f \equiv 0$ in the sequel.

4.2 Circular inclusion

The second benchmark example from the literature models a rigid circular inclusion in an infinite plate for the domain Ω with rather mixed boundary conditions indicated with mechanical symbols in Fig. 2. The exact solution [23] to the model problem (1) reads (with polar coordinates (r, ϕ) and $\kappa = 3 - 4\nu$, $\gamma = 2\nu - 1$, $a = 1/4$)

$$u_r = \frac{1}{8\mu r} \left((\kappa - 1)r^2 + 2\gamma a^2 + \left(2r^2 - \frac{2(\kappa + 1)a^2}{\kappa} + \frac{2a^4}{\kappa r^2} \right) \cos(2\phi) \right),$$

$$u_\phi = -\frac{1}{8\mu r} \left(2r^2 - \frac{2(\kappa - 1)a^2}{\kappa} - \frac{2a^4}{\kappa r^2} \right) \sin(2\phi).$$
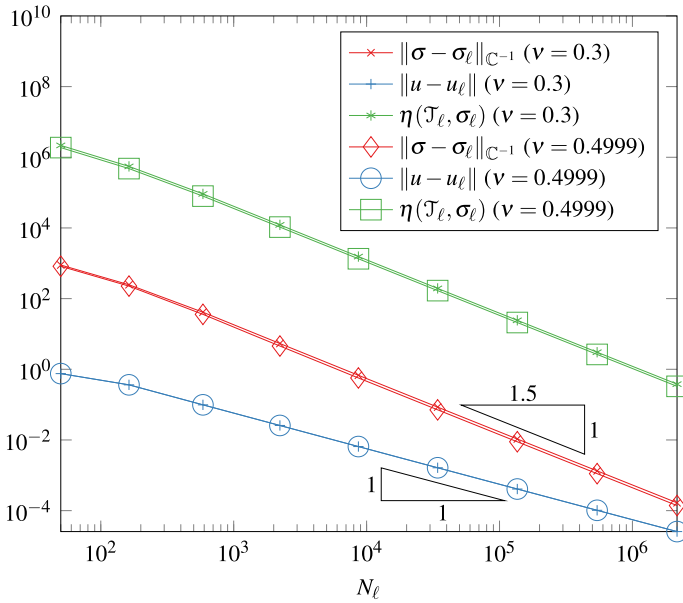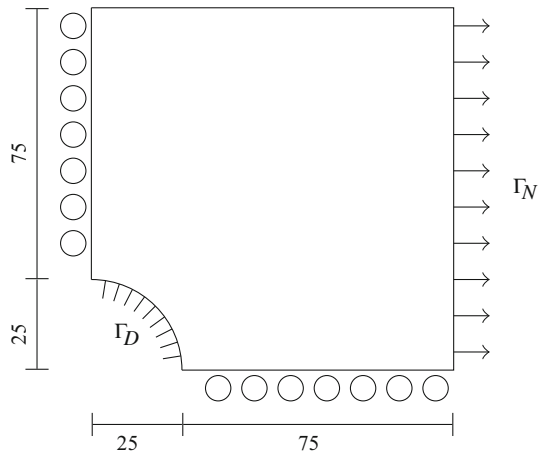
Fig. 1 Convergence history plot in academic example

Fig. 2 Domain circular inclusion

The approximation of the circular inclusion through a polygon is rather critical for the higher-order Arnold–Winther MFEM. In the absence of an implementation of parametric boundaries, adaptive mesh refinement is necessary for higher improvements. The adaptive algorithm of this section is the same for all examples and acts on polygons; in particular, it does not monitor the curved boundary, but whenever some edge at the curved part Γ_D is refined in this example, the midpoint is a new node and projected onto Γ_D. The convergence history plot in Fig. 3 shows a reduced convergence for uniform refinement, while adaptive refinement (of the circular boundary) leads to optimal third-order convergence.
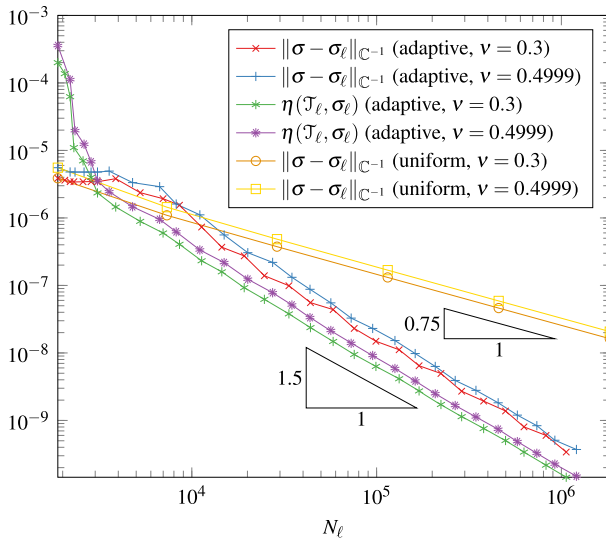
Fig. 3 Convergence history plot in circular inclusion benchmark

4.3 L-shaped benchmark

Consider the rotated L-shaped domain with Dirichlet and Neumann boundary depicted in Fig. 4. The exact solution reads in polar coordinates

$$u_r(r, \phi) = \frac{r^\alpha}{2\mu} \left(-(\alpha + 1) \cos((\alpha + 1)\phi) + (C_2 - \alpha - 1) C_1 \cos((\alpha - 1)\phi) \right),$$

$$u_\phi(r, \phi) = \frac{r^\alpha}{2\mu} \left((\alpha + 1) \sin((\alpha + 1)\phi) + (C_2 + \alpha - 1) C_1 \sin((\alpha - 1)\phi) \right).$$

The constants are $C_1 := -\cos((\alpha+1)\omega)/\cos((\alpha-1)\omega)$ and $C_2 := 2(\lambda+2\mu)/(\lambda+\mu)$, where $\alpha = 0.544483736782$ is the first root of $\alpha \sin(2\omega) + \sin(2\omega\alpha) = 0$ for $\omega = 3\pi/4$. The volume force $f \equiv 0$ and the Neumann boundary data $g \equiv 0$ vanish, and the Dirichlet boundary conditions u_D are extracted from the exact solution.

Figure 5 shows suboptimal convergence $\mathcal{O}(N_\ell^{-0.27})$, namely an expected rate α in terms of the maximal mesh-size, for uniform and fourth-order L^2 stress convergence for adaptive mesh-refinement.

Despite the singular solution, the adaptive algorithm recovers the higher convergence of Theorem 5 as in [15].

4.4 Cook membrane problem

One of the more popular benchmarks in computational mechanics is the tapered panel Ω with the vertices A, B, C, D of Fig. 6 clamped on the left side $\Gamma_D = \text{conv}(D, A)$ (with $u_D \equiv 0$) under no volume force ($f \equiv 0$) but applied surface tractions $g = (0, 1)$ along $\text{conv}(B, C)$ and traction free on the remaining parts $\text{conv}(A, B)$ and $\text{conv}(C, D)$ along the Neumann boundary.
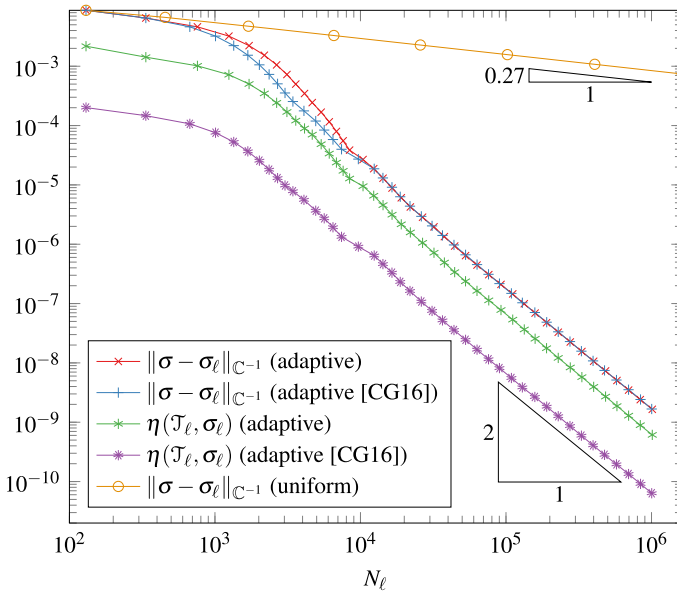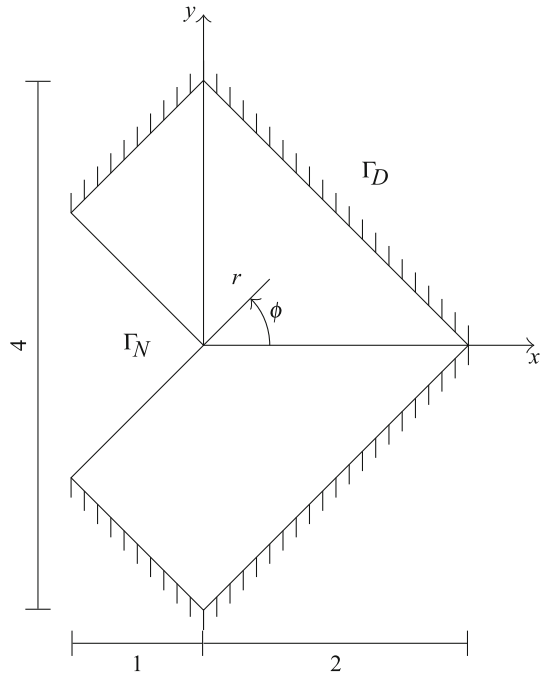
Fig. 4 L-shaped domain

Fig. 5 Convergence history plot in L-shaped benchmark for $\nu = 0.4999$

This example is a particular difficult one for the Arnold–Winther MFEM because of the incompatible Neumann boundary conditions on the right corners [12,15,16]. That means, although g is piecewise constant, g does not belong to $G(\mathcal{T})$ for
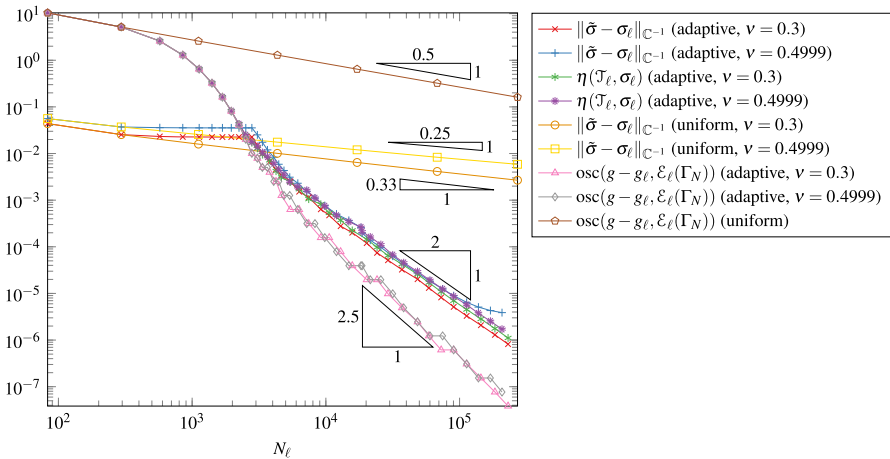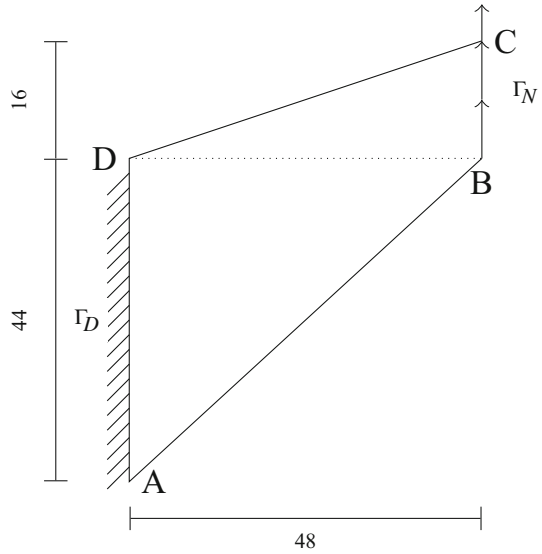
Fig. 6 Cook membrane

Fig. 7 Convergence history plot in Cook's membrane benchmark

any triangulation. In the two Neumann corner vertices B and C we therefore strongly impose the values $\sigma_\ell(B) = (0.2491, 0.7283; 0.7283, 0.6676)$ and $\sigma_\ell(C) = (3/20, 11/20; 11/20, 11/60)$ for the design of $g_\ell \in G(\mathcal{T}_\ell)$.

Since the exact solution is unknown, the error approximation rests on a reference solution $\tilde{\sigma}$ computed as $P_5(\mathcal{T})$ displacement approximation on the uniform refinement of the finest adapted triangulation.

The large pre-asymptotic range of the convergence history plot in Fig. 7 illustrates the difficulties of the Arnold–Winther finite element method in case of incompatible Neumann boundary conditions according to its nodal degrees of freedom. Once the resulting and dominating boundary oscillations (caused by the necessary choice of
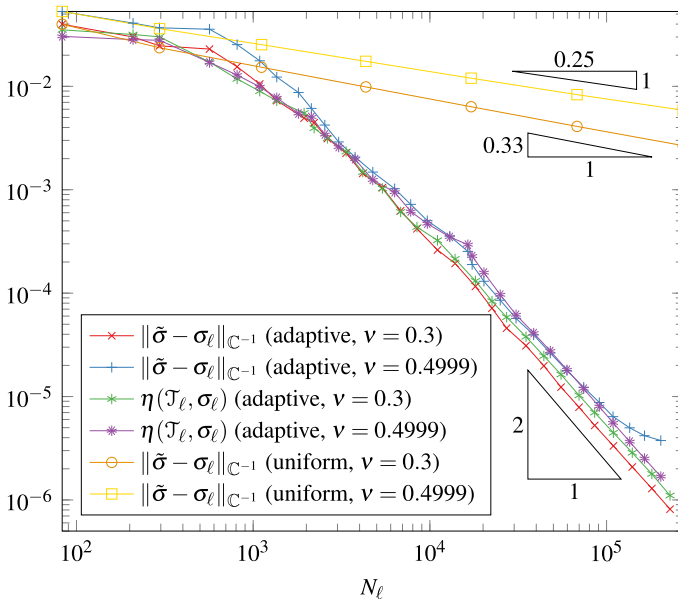
Fig. 8 Convergence history plot in Cook's membrane benchmark with modifications near the right corner points

discrete compatible Neumann conditions in $G(\mathcal{T}_\ell))\operatorname{osc}(g - g_\ell, \mathcal{E}_\ell(\Gamma_N))$ are resolved through adaptive mesh-refining, even the fourth-order L^2 stress convergence is visible in a long asymptotic range in (the approximated error and) the equivalent error estimator.

This example underlines that adaptive mesh-refining is unavoidable in computational mechanics with optimal rates and a large saving in computational time and memory compared to naive uniform mesh-refining.

With the modifications of the Arnold-Winter MFEM for incompatible Neumann data as outlined in Appendix B, which only involves adjustments of the right-hand side at the critical incompatible nodal stress degrees of freedom, we observe optimal convergence rates from the very beginning in Fig. 8 without any visible pre-asymptotically reduced convergence caused by incompatible Neumann boundary conditions.

4.5 Comments

The generic constants in this paper are not worked out explicitly in detail and so a numerical comparison with the earlier paper [15] cannot be quantitatively. It is conjectured that the residual-based error estimation with the reliability constants (for a guaranteed upper error bound) overestimates the true error up to an order of magnitude.

The qualitative comparison in Fig. 5 (without the reliability constants for the estimators) provides numerical evidence that the error estimators of this paper converge with the same convergence rates as those from [15] and it also indicates global equivalence of the errors with the two error estimators. The theoretical evidence in [15] for

efficiency depends on unrealistically high regularity assumptions – unlike the general efficiency results of this paper.

A Fourth-order convergence of the stress in L^2

This appendix explains a high-order convergence phenomenon observed in some numerical benchmark examples for the lowest-order Arnold–Winther method. Adopt the notation from this paper for $k = 1$ and let σ solve (1) and let $\sigma_h \in AW_k(\mathcal{T})$ solve (3).

Theorem 5 (fourth-order convergence) *Suppose $f = f_h \in P_1(\mathcal{T}; \mathbb{R}^2)$ and $g = g_h \in G(\mathcal{T})$ and suppose that the stress $\sigma \in H^4(\Omega; \mathbb{S})$. Then the L^2 stress error satisfies (with the maximal mesh-size h)*

$$\|\sigma - \sigma_h\|_{L^2(\Omega)} \lesssim h^4 \|\sigma\|_{H^4(\Omega)}.$$

Proof Since the stress error $\sigma - \sigma_h \in H^4(\mathcal{T}; \mathbb{S})$ is divergence-free, α vanishes in (7) and $\sigma - \sigma_h = \mathrm{Curl}^2 \beta \in H^4(\mathcal{T}; \mathbb{S})$. Since $\beta \in H^2(\mathcal{T})$ is piecewise in C^2, it follows $\beta \in C^1(\overline{\Omega})$. The Arnold–Winther finite elements have nodal degrees of freedom at the vertices and hence σ_h is continuous at each vertex $z \in \mathcal{N}$. Hence the second derivatives of $\beta \in C^2(\mathcal{T}) \cap C^1(\overline{\Omega})$ are continuous at each vertex $z \in \mathcal{N}$. It follows that the nodal interpolation operator I_A associated to the Argyris finite element space $A(\mathcal{T}) \subset C^1(\Omega) \cap P_5(\mathcal{T})$ exists for β in the classical sense and is composed of the piecewise local interpolation. This defines $\beta_h = I_A \beta$ and the divergence-free $\tau_h := \mathrm{Curl}^2 \beta_h \in AW_k(\mathcal{T})$ test function in (1) and in (3). Consequently,

$$\|\sigma - \sigma_h\|^2_{L^2(\Omega)} = (\sigma - \sigma_h, \mathrm{Curl}^2(\beta - \beta_h))_{L^2(\Omega)} \leq \|\sigma - \sigma_h\|_{L^2(\Omega)} |\beta - I_A\beta|_{H^2(\Omega)}.$$

This and standard local interpolation error estimates for the nodal interpolation of the quintic Argyris finite elements [7,8,20] show

$$\|\sigma - \sigma_h\|_{L^2(\Omega)} \lesssim h^4 |\beta|_{H^6(\mathcal{T})} = h^4 |\sigma|_{H^4(\Omega)}.$$

(With $\sigma - \sigma_h = \mathrm{Curl}^2 \beta$ and $|\sigma_h|_{H^4(\mathcal{T})} = 0$ for piecewise cubic σ_h in the last step.) □

B General Neumann data

The nodal degrees of freedom of the Arnold–Winther stresses do not allow a nodal interpolation of arbitrary Neumann data. As documented in [15,16] the performance of the numerical method indeed suffers from that property.

In this work, the following alternative is proposed. Let $g \in L^2(\Gamma; \mathbb{R}^2)$ be the Neumann data. Define $g_h := \Pi_{k+2}^{\Gamma} g$ where Π_{k+2}^{Γ} denotes the L^2 projection onto $P_{k+2}(\mathscr{E}(\Gamma); \mathbb{R}^2)$. Note that g_h may be discontinuous. Let $\sigma^P \in H(\text{div}, \Omega; \mathbb{S})$ be any piecewise polynomial stress approximation with $\sigma^P = g_h$ on Γ_N. The explicit design of such a particular solution is outlined in Appendix C below.

The proposed scheme is to seek a solution $\sigma_h^0 \in \Sigma(0, \mathscr{T})$ and $u_h \in V_h$ such that, for all $\tau_h \in \Sigma(0, \mathscr{T})$ and all $v_h \in V_h$,

$$\int_{\Omega} \sigma_h^0 : \mathbb{C}^{-1} \tau_h \, dx + \int_{\Omega} u_h \cdot \text{div} \, \tau_h \, dx = \int_{\Gamma_D} u_D \cdot (\tau_h v) \, ds - \int_{\Omega} \sigma^P : \mathbb{C}^{-1} \tau_h \, dx$$

$$\int_{\Omega} v_h \cdot \text{div} \, \sigma_h \, dx = - \int_{\Omega} (f + \text{div} \, \sigma^P) \cdot v_h \, dx. \tag{12}$$

Then $\sigma_h := \sigma_h^0 + \sigma^P$ satisfies the Neumann boundary conditions along Γ as well as $-\text{div} \, \sigma_h = f$ in Ω. Note that this modification merely affects the right-hand side while the system matrix remains unchanged.

The scheme allows for a direct a priori error analysis. The following result states a quasi-optimal a priori error estimate provided σ^P is chosen sufficiently accurate.

Theorem 6 (a priori error estimate) *The discrete solution (σ_h, u_h) to the modified scheme* (12) *satisfies*

$$\|\sigma - \sigma_h\|_{\mathbb{C}^{-1}} \lesssim \inf_{\sigma_h^\star \in \Sigma(0, \mathscr{T})} \left(\|\sigma - \sigma_h^\star - \sigma^P\|_{\mathbb{C}^{-1}} + \|\Pi_k(f + \text{div}(\sigma_h^\star + \sigma^P))\| \right).$$

Proof The discrete inf-sup condition (with appropriate discrete test functions $\tau_h \in \Sigma(0, \mathscr{T})$ and $v_h \in V_h$ with norm 1) and the discrete equations (12) show that, for any $\sigma_h^\star \in \Sigma(0, \mathscr{T})$,

$$\|\sigma_h^\star - \sigma_h^0\|_{\mathbb{C}^{-1}} + \|\text{div}(\sigma_h^\star - \sigma_h^0)\| + \|u_h - \Pi_k u\|$$
$$\lesssim (\sigma_h^\star - \sigma_h^0, \mathbb{C}^{-1} \tau_h)_{L^2(\Omega)} + (\text{div}(\sigma_h^\star - \sigma_h^0), v_h)_{L^2(\Omega)} + (\text{div} \, \tau_h, u_h - \Pi_k u)_{L^2(\Omega)}$$
$$= (\sigma_h^\star + \sigma^P - \sigma, \mathbb{C}^{-1} \tau_h)_{L^2(\Omega)} + (\Pi_k(\text{div} \, \sigma_h^\star + f + \text{div} \, \sigma^P), v_h)_{L^2(\Omega)}$$
$$\leq \|\sigma - \sigma_h^\star - \sigma^P\|_{\mathbb{C}^{-1}} + \|\Pi_k(f + \text{div}(\sigma_h^\star + \sigma^P))\|.$$

The decomposition $\sigma_h = \sigma_h^0 - \sigma_P$ and the triangle inequality

$$\|\sigma - \sigma_h\|_{\mathbb{C}^{-1}} \leq \|\sigma - \sigma_h^\star - \sigma^P\|_{\mathbb{C}^{-1}} + \|\sigma_h^\star - \sigma_h^0\|_{\mathbb{C}^{-1}}$$

thus imply the stated bound. □

The a posteriori error estimates from Theorem 1, Sects. 2 and 3 hold verbatim also for this case. For the efficiency proof it is required that σ^P is piecewise polynomial. Appendix C proposes an explicit design as a discrete particular solution.

C Neumann boundary conditions

This section explains the modification of the lowest-order Arnold–Winther finite element methods that requires a different treatment of the nodal degrees of freedom at a vertex z on the Neumann boundary Γ_N in the presence of incompatible Neumann data.

Two situations arise at the vertex $z \in \mathcal{N}$ in the relative interior of Γ_N with neighboring triangles $\mathcal{T}(z) := \{T \in \mathcal{T} : z \in \mathcal{N}(T)\} =: \{T_1, \ldots, T_J\}$ enumerated counterclockwise. For $J = 1$ there is no option to modify nodal degrees of freedom to allow for incompatible Neumann boundary conditions at the vertex z and one requires $J \geq 2$ (resp. $J \geq 3$) in case the angle at the polygon Γ_N is different from π (resp. equal to π). The idea behind the required modification of the Arnold–Winther finite element space $AW_k(\mathcal{T})$ is to split the various degrees of freedom $\sigma_{AW}|_{T_j}(z) \in \mathbb{S}$ for $j = 1, \ldots, J$, which coincide in $AW_k(\mathcal{T})$. This modification leads to some conforming and piecewise Arnold–Winther space $AW'_k(\mathcal{T}) \subset H(\mathrm{div}, \Omega; \mathbb{S})$ and its modified finite element space

$$\Sigma'(g_h, \mathcal{T}) := \Sigma(\Pi_k g) \cap AW'_k(\mathcal{T})$$

for the edgewise L^2 projection $\Pi_k g$ of the Neumann data g.

Two triangles at an interior vertex of the Neumann boundary

In the first part suppose that $J = 2$ and that the node z is a vertex of the polygon Γ_N with an interior angle $\omega_1 + \omega_2 \neq \pi$ for the interior angle ω_j of the triangle T_j at the vertex z. Let α denote the angle of the edge $E_1 \subset \overline{\Gamma_N}$ in the global coordinate system, so that the interior edge E_2 shared by T_1 and T_2 has the angle $\varphi := \alpha + \omega_1$, while the remaining edge $E_3 \subset \overline{\Gamma_N}$ has the angle $\beta = \alpha + \omega_1 + \omega_2$; the respective normals ν_{E_1}, ν_{E_2}, and $-\nu_{E_3}$ read $(\sin(\psi), -\cos(\psi))$ for $\psi = \alpha, \varphi$, and β; ν_{E_1} and ν_{E_3} point outwards of the domain.

Let $(\sigma_{11}^{(j)}, \sigma_{12}^{(j)}, \sigma_{22}^{(j)})$ denote the three components of $\sigma'_{AW}|_{T_j}(z) \in \mathbb{S}$ for $j = 1, 2$. Those six variables (rather then three $\sigma_{11}^{(1)} = \sigma_{11}^{(2)}$ etc. for the classical nodal values of AW) are required to satisfy boundary conditions

$$\sigma'_{AW}|_{T_1}(z)\nu_{E_1} = \Pi_k(g|_{E_1})(z) \quad \text{and} \quad \sigma'_{AW}|_{T_2}(z)\nu_{E_3} = \Pi_k(g|_{E_3})(z)$$

and, for $H(\mathrm{div}, \Omega; \mathbb{S})$-conformity, the interface conditions

$$\sigma'_{AW}|_{T_1}(z)\nu_{E_2} = \sigma'_{AW}|_{T_2}(z)\nu_{E_2}.$$

This 6×6 linear system of equations has a unique solution (despite of possibly incompatible conditions provided by $\Pi_k(g|_{E_1})(z)$ and $\Pi_k(g|_{E_3})(z)$). The proof requires the regularity of the corresponding 6×6 coefficient matrix

$$
\begin{pmatrix}
\sin\alpha & -\cos\alpha & 0 & & & \\
0 & \sin\alpha & -\cos\alpha & & & \\
\sin\varphi & -\cos\varphi & 0 & -\sin\varphi & \cos\varphi & 0 \\
0 & \sin\varphi & -\cos\varphi & 0 & -\sin\varphi & \cos\varphi \\
& & & -\sin\beta & \cos\beta & 0 \\
& & & 0 & -\sin\beta & \cos\beta
\end{pmatrix}
$$

with empty space representing 2×3 zero blocks, which is multiplied with the coefficient vector

$$
(\sigma_{11}^{(1)}, \sigma_{12}^{(1)}, \sigma_{22}^{(1)}, \sigma_{11}^{(2)}, \sigma_{12}^{(2)}, \sigma_{22}^{(2)}) \in \mathbb{R}^6
$$

representing $(\sigma'_{AW}|_{T_1}, \sigma'_{AW}|_{T_2})$ at z.

There are several ways to cross-check the regularity of this coefficient matrix. One reduces it to the regularity of the 3×3 matrix

$$
\begin{pmatrix}
\cos^2\alpha & \sin\alpha\,\cos\alpha & \sin^2\alpha \\
\cos^2\varphi & \sin\varphi\,\cos\varphi & \sin^2\varphi \\
\cos^2\beta & \sin\beta\,\cos\beta & \sin^2\beta
\end{pmatrix}
$$

as follows. The following abbreviations apply throughout this section

$$
m(\psi) := (\cos^2\psi, \sin\psi\,\cos\psi, \sin^2\psi)^T \quad \text{and} \quad N(\psi) := \begin{pmatrix} \sin\psi & -\cos\psi & 0 \\ 0 & \sin\psi & -\cos\psi \end{pmatrix}.
$$

Any vector $(x_1, \ldots, x_6)$ in the kernel of the above displayed 6×6 coefficient matrix satisfies in particular $N(\alpha)(x_1, x_2, x_3)^T = 0 \in \mathbb{R}^2$. Hence it is parallel to the cross-product of the two row vectors in the 2×3 matrix $N(\alpha)$ and so $(x_1, x_2, x_3)^T \| m(\alpha)$. The same is true for $(x_4, x_5, x_6)^T \| m(\beta)$. The remaining two conditions for $(x_1, \ldots, x_6)$ to be a kernel vector read $N(\varphi)(x_4 - x_1, x_5 - x_2, x_6 - x_3)^T = 0 \in \mathbb{R}^2$ and so $(x_4 - x_1, x_5 - x_2, x_6 - x_3) \| m(\varphi)$. This leads to $(x_1, \ldots, x_6) = 0 \in \mathbb{R}^6$ if and only if the displayed 3×3 matrix $(m(\alpha), m(\varphi), m(\beta))^T \in \mathbb{R}^{3\times 3}$ is regular. Its determinant det depends on ω_1 and ω_2 and not on α if one substitutes $\varphi := \alpha + \omega_1$ and $\beta := \alpha + \omega_1 + \omega_2$; the elementary proof abbreviates the Vandermonde determinant

$$
\det =: \begin{vmatrix} \cos^2 & \sin\cos & \sin^2 \\ \alpha & \varphi & \beta \end{vmatrix}
$$

of a 3×3 matrix with columns determined by the three functions $\cos^2$, $\sin\cos$, $\sin^2$ and rows evaluated respectively at α, φ, β. The derivative $\partial \det /\partial\alpha$ of the determinant det with respect to the variable reads

$$
\begin{vmatrix} -2\sin\cos & \sin\cos & \sin^2 \\ \alpha & \varphi & \beta \end{vmatrix} + \begin{vmatrix} \cos^2 & \cos^2 - \sin^2 & \sin^2 \\ \alpha & \varphi & \beta \end{vmatrix} + \begin{vmatrix} \cos^2 & \sin\cos & 2\sin\cos \\ \alpha & \varphi & \beta \end{vmatrix}.
$$

Each of these three determinants vanishes (for the columns are linearly dependent). This proves that $\partial \det / \partial \alpha = 0$ and so one may choose without loss of generality $\alpha = 0$ to compute

$$\det = \sin(\omega_1) \sin(\omega_2) \sin(\omega_1 + \omega_2).$$

Since $\beta - \alpha = \omega_1 + \omega_2 \neq \pi$, $\det \neq 0$ and the design of a minimum norm solution of the above six conditions is feasible for any (in particular incompatible) discrete data.

Provided the angle at a node in the relative interior of the Neumann boundary is π, the design of this subsection may be infeasible (although solutions exist for discrete compatible data) and $J \geq 3$ is required.

Three triangles at a node in the Neumann boundary

Suppose $\mathcal{T}(z) = \{T_1, T_2, T_3\}$ enumerated counterclockwise with interior angles $\omega_1, \omega_2, \omega_3$ at the vertex z and E_1 parallel to E_4 on $\overline{\Gamma_N}$ and $\omega_1 + \omega_2 + \omega_3 = \pi$ with $\beta = \alpha + \pi$. Let $(\sigma_{11}^{(j)}, \sigma_{12}^{(j)}, \sigma_{22}^{(j)})$ denote the three components of $\sigma_{AW}'|_{T_j}(z) \in \mathbb{S}$ for $j = 1, 2, 3$. With the aforementioned block matrices, the four Neumann boundary conditions and the four interface conditions for $H(\text{div}, \Omega; \mathbb{S})$-conformity can be summarized into a linear system of equations with the 8×9 coefficient matrix

$$\begin{pmatrix} N(\alpha) & & \\ N(\alpha + \omega_1) & -N(\alpha + \omega_1) & \\ & N(\alpha + \omega_1 + \omega_2) & -N(\alpha + \omega_1 + \omega_2) \\ & & N(\alpha) \end{pmatrix}.$$

In order to prove that the design of $(\sigma_{11}^{(1)}, \sigma_{12}^{(1)} \ldots, \sigma_{22}^{(3)}) \in \mathbb{R}^9$ is always possible (even for incompatible discrete Neumann data), it suffices to prove that this coefficient matrix has full rank. The subsequent regular transformation matrix

$$T := \begin{pmatrix} -\sin \alpha & -\cos \alpha & \cos^2 \alpha \\ \cos \alpha & -\sin \alpha & \sin \alpha \cos \alpha \\ \sin \alpha & \cos \alpha & \sin^2 \alpha \end{pmatrix}$$

leads to a new set of variables $(\tau_{11}^{(1)}, \tau_{12}^{(1)} \ldots, \tau_{22}^{(3)}) \in \mathbb{R}^9$ by $(\sigma_{11}^{(j)}, \sigma_{12}^{(j)}, \sigma_{22}^{(j)})^T := T(\tau_{11}^{(j)}, \tau_{12}^{(j)}, \tau_{22}^{(j)})^T$ for $j = 1, 2, 3$. Elementary trigonometry shows

$$\widetilde{N}(\psi - \alpha) := N(\psi)T = \begin{pmatrix} -\cos(\psi - \alpha) & -\sin(\psi - \alpha) & \cos \alpha \sin(\psi - \alpha) \\ \sin(\psi - \alpha) & -\cos(\psi - \alpha) & \sin \alpha \sin(\psi - \alpha) \end{pmatrix}.$$

In particular, $-N(\alpha)T$ is the unit matrix and shows that the kernel vectors $(\tau_{11}^{(1)}, \tau_{12}^{(1)} \ldots, \tau_{22}^{(3)}) \in \mathbb{R}^9$ of the aforementioned 8×9 coefficient matrix satisfy $\tau_{11}^{(j)} = 0 = \tau_{12}^{(j)}$ for $j = 1$ and $j = 3$. Moreover, the remaining components $\tau_{22}^{(1)}, \tau_{11}^{(2)}, \tau_{12}^{(2)}, \tau_{22}^{(2)}$, and $\tau_{22}^{(3)}$ of a (transformed) kernel vector satisfy

$$
\begin{pmatrix}
\cos(\omega_1) & \sin(\omega_1) & -2\cos\alpha\,\sin(\omega_1) & -\cos\alpha\,\sin(\omega_1) \\
-\sin(\omega_1) & \cos(\omega_1) & -2\sin\alpha\,\sin(\omega_1) & -\sin\alpha\,\sin(\omega_1) \\
-\cos(\omega_1+\omega_2) & -\sin(\omega_1+\omega_2) & \cos\alpha\,\sin(\omega_1+\omega_2) & 2\cos\alpha\,\sin(\omega_1+\omega_2) \\
\sin(\omega_1+\omega_2) & -\cos(\omega_1+\omega_2) & \sin\alpha\,\sin(\omega_1+\omega_2) & 2\sin\alpha\,\sin(\omega_1+\omega_2)
\end{pmatrix}
\begin{pmatrix}
\tau_{11}^{(2)} \\
\tau_{12}^{(2)} \\
\tau_{22}^{(2)} - \tau_{22}^{(1)} \\
\tau_{22}^{(2)} - \tau_{22}^{(3)}
\end{pmatrix}
= 0.
$$

It remains to prove that the determinant of this 4×4 coefficient matrix is nonzero, because this proves $\tau_{11}^{(2)} = 0 = \tau_{12}^{(2)}$ and $\tau_{22}^{(1)} = \tau_{22}^{(2)} = \tau_{22}^{(3)}$ and so the null space is one-dimensional and the rank of the above 8×9 matrix is 8, i.e., all conditions can be satisfied by a one-dimensional (whence non-empty) solution space.

The expansion of the determinant of the 4×4 coefficient matrix confirms that the determinant is equal to $-3\sin(\omega_1)\sin(\omega_2)\sin(\omega_1+\omega_2)$ and so negative for $0 < \omega_1 < \omega_1 + \omega_2 < \pi$.

More triangles at a node in the Neumann boundary

The general situation is that there are $J \geq 2$ (resp. $J \geq 3$) triangles at a node $z \in \Gamma_N$ in the relative interior of the Neumann boundary Γ_N with an interior angle $\neq \pi$ (resp. $= \pi$) of the polygon Γ_N at z. The above analysis shows that the modified Arnold–Winther space $AW_k'(\mathcal{T}) \subset H(\mathrm{div}, \Omega; \mathbb{S})$ allows for solutions for $J = 2$ (resp. $J = 3$). In case that J is larger, one may choose a partition of $T_1, \ldots, T_J$ in two (resp. three) groups $T_1, \ldots, T_k, T_{k+1}, \ldots T_J$ (resp. $T_1, \ldots, T_k, T_{k+1}, \ldots, T_\ell, T_{\ell+1}, \ldots T_J$). Then the extra constraint $\sigma_{AW}'|_{T_1} = \ldots = \sigma_{AW}'|_{T_k}$ and $\sigma_{AW}'|_{T_{k+1}} = \ldots = \sigma_{AW}'|_{T_J}$ for each group reduces the discussion to the above calculations with two triangles (resp. to the calculations with three triangles).

Modified Arnold–Winter FEM for Neumann boundary

The implementation of nodes at the Neumann boundary concerns only z in (the relative interior of) Γ_N in case of incompatible discrete Neumann data. The most general case may be implemented via Lagrange multipliers for the interface conditions of the nodal values of $\sigma_{AW}'|_{T_j}(z)$ in $AW_k'(\mathcal{T}) \subset H(\mathrm{div}, \Omega; \mathbb{S})$.

References

1. Alonso, A.: Error estimators for a mixed method. Numer. Math. **74**(4), 385–395 (1996)
2. Arnold, D.N.: Differential complexes and numerical stability. In: Proceedings of the International Congress of Mathematicians, Vol. I (Beijing, 2002), pp. 137–157. Higher Ed. Press, Beijing (2002)
3. Arnold, D.N., Brezzi, F., Douglas, J.: PEERS: a new mixed finite element for plane elasticity. Jpn. J. Appl. Math. **1**, 347–367 (1984)
4. Arnold, D.N., Falk, R.S., Winther, R.: Finite element exterior calculus, homological techniques, and applications. Acta Numer. **15**, 1–155 (2006)
5. Arnold, D.N., Winther, R.: Mixed finite elements for elasticity. Numer. Math. **92**(3), 401–419 (2002)
6. Boffi, D., Brezzi, F., Fortin, M.: Mixed Finite Element Methods and Applications. Springer Series in Computational Mathematics, vol. 44. Springer, Heidelberg (2013)
7. Braess, D.: Finite Elements. Theory, Fast Solvers, and Applications in Elasticity Theory, 3rd edn. Cambridge University Press, Cambridge (2007)

8. Brenner, S.C., Scott, L.R.: The Mathematical Theory of Finite Element Methods. Texts in Applied Mathematics, vol. 15, 3rd edn. Springer, New York (2008)
9. Carstensen, C.: A posteriori error estimate for the mixed finite element method. Math. Comput. **66**(218), 465–476 (1997)
10. Carstensen, C.: A unifying theory of a posteriori finite element error control. Numer. Math. **100**(4), 617–637 (2005)
11. Carstensen, C., Dolzmann, G.: A posteriori error estimates for mixed FEM in elasticity. Numer. Math. **81**(2), 187–209 (1998)
12. Carstensen, C., Eigel, M., Gedicke, J.: Computational competition of symmetric mixed FEM in linear elasticity. Comput. Methods Appl. Mech. Eng. **200**(41–44), 2903–2915 (2011)
13. Carstensen, C., Feischl, M., Page, M., Praetorius, D.: Axioms of adaptivity. Comput. Math. Appl. **67**(6), 1195–1253 (2014)
14. Carstensen, C., Gallistl, D., Schedensack, M.: L^2 best approximation of the elastic stress in the Arnold–Winther FEM. IMA J. Numer. Anal. **36**(3), 1096–1119 (2016)
15. Carstensen, C., Gedicke, J.: Robust residual-based a posteriori Arnold–Winther mixed finite element analysis in elasticity. Comput. Methods Appl. Mech. Eng. **300**, 245–264 (2016)
16. Carstensen, C., Günther, D., Reininghaus, J., Thiele, J.: The Arnold-Winther mixed FEM in linear elasticity. Part I: Implementation and numerical verification. Comput. Methods Appl. Mech. Eng. **197**, 3014–3023 (2008)
17. Carstensen, C., Hu, J.: A unifying theory of a posteriori error control for nonconforming finite element methods. Numer. Math. **100**(3), 473–502 (2007)
18. Carstensen, C., Peterseim, D., Schröder, A.: The norm of a discretized gradient in $H(\mathrm{div})^*$ for a posteriori finite element error analysis. Numer. Math. **132**, 519–539 (2016)
19. Carstensen, C., Rabus, H.: Axioms of adaptivity with separate marking for data resolution. SIAM J. Numer. Anal. **55**(6), 2644–2665 (2017)
20. Ciarlet, P.G.: The Finite Element Method for Elliptic Problems. Studies in Mathematics and Its Applications, vol. 4. North-Holland Publishing Co., Amsterdam-New York-Oxford (1978)
21. Girault, V., Scott, L.R.: Hermite interpolation of nonsmooth functions preserving boundary conditions. Math. Comput. **71**(239), 1043–1074 (2002)
22. Huang, J., Huang, X., Xu, Y.: Convergence of an adaptive mixed finite element method for Kirchhoff plate bending problems. SIAM J. Numer. Anal. **49**(2), 574–607 (2011)
23. Kouhia, R., Stenberg, R.: A linear nonconforming finite element method for nearly incompressible elasticity and Stokes flow. Comput. Methods Appl. Mech. Eng. **124**(3), 195–212 (1995)
24. Verfürth, R.: A Review of a Posteriori Error Estimation and Adaptive Mesh-Refinement Techniques. Wiley, Hoboken (1996)